



Review

# Advances in Hole Transport Materials for Layered Casting Solar Cells

Vu Khac Hoang Bui <sup>1</sup>  and Thang Phan Nguyen <sup>2,\*</sup> 

<sup>1</sup> Department of Environment and Energy, Sejong University, Seoul 05006, Republic of Korea; buikhachoangvu@sejong.ac.kr

<sup>2</sup> Department of Chemical and Biological Engineering, Gachon University, Seongnam-si 13120, Gyeonggi-do, Republic of Korea

\* Correspondence: npthang@gachon.ac.kr

**Abstract:** Huge energy consumption and running out of fossil fuels has led to the advancement of renewable sources of power, including solar, wind, and tide. Among them, solar cells have been well developed with the significant achievement of silicon solar panels, which are popularly used as windows, rooftops, public lights, etc. In order to advance the application of solar cells, a flexible type is highly required, such as layered casting solar cells (LCSCs). Organic solar cells (OSCs), perovskite solar cells (PSCs), or dye-sensitive solar cells (DSSCs) are promising LCSCs for broadening the application of solar energy to many types of surfaces. LCSCs would be cost-effective, enable large-scale production, are highly efficient, and stable. Each layer of an LCSC is important for building the complete structure of a solar cell. Within the cell structure (active material, charge carrier transport layer, electrodes), hole transport layers (HTLs) play an important role in transporting holes to the anode. Recently, diverse HTLs from inorganic, organic, and organometallic materials have emerged to have a great impact on the stability, lifetime, and performance of OSC, PSC, or DSSC devices. This review summarizes the recent advances in the development of inorganic, organic, and organometallic HTLs for solar cells. Perspectives and challenges for HTL development and improvement are also highlighted.

**Keywords:** polymer solar cells; perovskite solar cell; hole transport layer; inorganic HTL; organic HTL



**Citation:** Bui, V.K.H.; Nguyen, T.P. Advances in Hole Transport Materials for Layered Casting Solar Cells. *Polymers* **2023**, *15*, 4443. <https://doi.org/10.3390/polym15224443>

Academic Editor: Yung-Sheng Yen

Received: 16 October 2023

Revised: 7 November 2023

Accepted: 15 November 2023

Published: 17 November 2023



**Copyright:** © 2023 by the authors. Licensee MDPI, Basel, Switzerland. This article is an open access article distributed under the terms and conditions of the Creative Commons Attribution (CC BY) license (<https://creativecommons.org/licenses/by/4.0/>).

## 1. Introduction

Perovskite solar cells (PSCs), dye-sensitive solar cells (DSSCs), and polymer solar cells (PSCs) are examples of layered casting solar cells (LCSCs). PSCs are a particular kind of solar cell that use lead- or tin halide-based materials with perovskite structures as their light-harvesting active layer [1,2]. The power conversion efficiency (PCE) of lab-scale PSCs has grown from 3.8% in 2009 to 26.1% in 2023 for single-junction structures and 29.8% for silicon-based tandem structures [1,3–6]. Perovskite solar cells have drawn a lot of research attention because of their promise for high efficiency, affordable manufacturing, and compatibility with a variety of device topologies [7,8]. Ongoing research is focused on addressing challenges related to stability, scalability, and toxicity concerns associated with lead-based perovskites [7,8]. Organic photovoltaics (OPVs), commonly referred to as organic solar cells (OSC), are a subclass of LCSCs for which the active layer for converting sunlight into energy is made of organic components. OSCs offer advantages such as flexibility, lightweight design, and the potential for low-cost fabrication through solution-based processes [9–11]. The performance and efficiency of OSCs depend on the choice of donor and acceptor materials, as well as the morphology of the active layer, which can be optimized through processing techniques. While they typically have lower efficiency compared to inorganic solar cells, ongoing research aims to improve their performance and commercial viability [9–11]. DSSCs consist of a porous semiconductor film (usually titanium dioxide, TiO<sub>2</sub>) coated with a light-absorbing dye, an electrolyte solution, and

a counter electrode. The dye absorbs photons and generates excited electrons, which are introduced into the semiconductor material. These electrons are then collected at the electrode, creating an electric current [12,13]. In general, both perovskite and organic solar cells have their own unique advantages and challenges. Perovskites solar cells have shown remarkable efficiency improvements but need further development in terms of stability. Meanwhile, OGCs have advantages in terms of flexibility and lightweight design, but efficiency and stability improvements are ongoing research goals. DSSCs, while having lower efficiency compared to other types of solar cells, offer advantages in low light or under artificial conditions [12,13].

LCSCs have various advantages compared to conventional solar cells. LCSCs can collect more sunlight by using different materials with different band gaps and absorption spectra. LCSCs can be more efficient by reducing thermalization losses, increasing open-circuit voltage, and improving charge separation. By using cheaper or more abundant materials, such as organic polymers or perovskites, and simpler fabrication methods, such as solution processing or hot casting, LCSCs have lower fabrication costs [12,14,15]. However, in general, LCSCs still maintain some limitations. LCSCs have poor stability due to the degradation of materials, interfacial defects, moisture sensitivity, or thermal stress. It is difficult to optimize LCSCs due to the interplay of different layers, the trade-off between current and voltage, and the compatibility of different materials. Lastly, the environmental issue remains due to the application of toxic or scarce materials (lead or indium) and the generation of waste or emissions during production [12,14,15].

Charge separation in solar cells relies on the generation of electron–hole pairs upon photo absorption, the creation of an electric field within the semiconductor material, and the motion of charged carriers to their respective region [12,16]. The separated electrons and holes travel through an external circuit to power electrical devices or charge a battery [12,16]. In many LCSCs, including perovskite solar cells and organic solar cells, a hole transport layer (HTL) is utilized to speed up the extraction and transportation of positive charge carriers (holes) from the active layer to the anode [8,14,17]. The HTL also serves as a barrier to stop electron leakage to the anode and as a layer of defense to shield the active layer from oxygen and moisture [8,14,17]. The HTL can be made of inorganic and organic materials, depending on the compatibility, cost, stability, and performance of the solar cells [14,17]. An ideal material for the HTL should have high hole mobility, excess holes, a relatively narrow bandgap, low defect density, good stability, and compatibility with other layers [8,18–20]. In this review, we focus on the recent progress of inorganic and organic HTLs in LCSCs, their advantages and disadvantages, and discuss the remaining challenges of each type of HTL that should be overcome in future studies.

## 2. Solar Cell Factors

A typical OSC is made up of an absorber, an electron transport layer (ETL), a hole transport layer (HTL), and anode and cathode electrodes [16]. One of the two electrodes is a substrate-compact transparent conducting oxide (TCO) electrode, which provides the conductive layer and allows most light to pass through. The TCO generally consists of indium tin oxide (ITO) or FTO (fluorine-doped tin oxide), the transparency of which is up to 93% [21]. An absorber is an organic/hybrid/inorganic semiconductor that can highly absorb light. It is also called an active material. In organic semiconductors, the lowest unoccupied molecular orbital (LUMO) and the highest occupied molecular orbital (HOMO) are the energy bands, which are similar to the conduction band (CB) and valence band (VB) of inorganic semiconductors, relating to electrons and holes as charge carriers, respectively. When light strikes the solar cell, the active material will absorb photons and form excitons (electron–hole couples) in the HOMO. The electrons and holes will immediately be separated to the LUMO and HOMO, respectively. Then, the ETL and HTL will transport charge carriers to the two electrodes, creating a different voltage potential for a solar cell. If the TCO is on the anode side, it is a conventional structure, and if it is on the cathode side, it is an inverted structure, as shown in Figure 1a. Therefore, the hole

can be collected from the front or back side of the cell, depending on the conventional or inverted structure, respectively. This structure will be determined by the casting layer technique or the properties of each layer. When irradiating light to an OSC, photoelectric conversion occurs, which includes three main processes: (I) light absorption and creation of excitons, (II) separation of excitons to electrons and holes, and (III) selective collection of charge carriers. An ideal OSC should have a good absorber, and the ETL and HTL should provide quick carrier transport to prevent the recombination of electrons and holes. In energy band expression, the layers of the OSC must follow the band alignment to optimize the carrier transport process, which is described in Figure 1b. Thus, the HTL is an electron-blocking material in addition to being a hole transport material. The ETL transports electrons and blocks holes. Later, more layer structures are established using separating hole/electron-blocking layers.

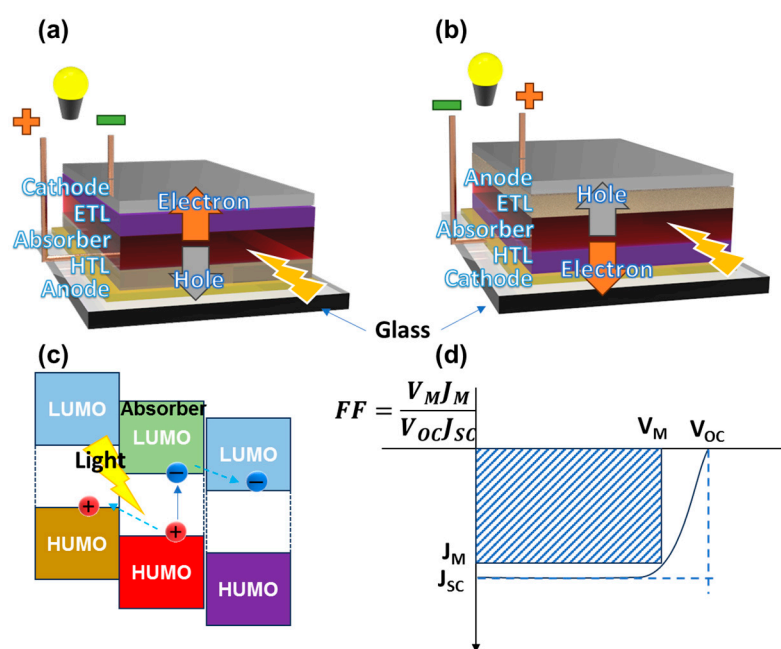


**Figure 1.** (a) Conventional and (b) inverted structures of an organic solar cell; (c) band gap alignment of active material with electron/hole transport; (d) current density ( $J$ )–voltage ( $V$ ) curves of the solar cell with the inset of the fill factor equation.

To evaluate a solar cell's performance, there are some major factors, including the fill factor (FF), power conversion efficiency (PCE), open-circuit voltage ( $V_{OC}$ ), and short-circuit current density ( $J_{SC}$ ). The PCE is calculated using the following equation:

$$PCE = \frac{V_{OC} \times J_{SC} \times FF}{P_I}$$

where  $P_I$  is the power density of incident light;  $V_{OC}$  is the highest voltage that the cell can supply; and  $J_{SC}$  is the highest current density for the output.

FF is the ratio of maximum power output to maximum obtainable power output ( $FF = P_{max} / (V_{OC} \times J_{SC})$ ), as shown in Figure 1c. Thus, FF indicates the quality of a solar cell, which is the obtainability of high current density and high voltage or output power. To obtain a standard measurement, solar cells are generally irradiated by a solar simulator light source with a power of  $1000 \text{ W m}^{-2}$ , and its light spectrum is equivalent to the light of AM 1.5 spectrum [22]. The PCE indicates how many percentages of incident light can be converted to an electric signal for output. The PCE depends much on the absorber and the efficiency of the charge transfer process by the ETL and HTL. A conventional cell with an ITO/PEDOT:PSS/P3HT:PC<sub>61</sub>BM/PC61BM/LiF/Al structure can exhibit a PCE of 3.0–4.0%.

If PC<sub>61</sub>BM is replaced by PC<sub>71</sub>BM, the PCE can be 7.0–8.0%, or by PTB7:PC<sub>71</sub>BM, the PCE can be 7.0–9.0%, etc. [23]. Therefore, when investigating the electron transport material (ETM) and hole transport material (HTM) in a solar cell, reference cells with or without a traditional ETM, such as PCBM, or HTM, such as PEDOT:PSS, should be prepared at the same time. In this study, the effect of various HTMs on solar cell performance will be revealed. The energy level, work function design, and surface engineering technique play important roles in achieving the reproducibility of organic layered solar cells.

### 3. Organic Hole Transport Layer (OHTL)

The organic hole transport layer (OHTL) is a layer of organic material that is used in LCSCs to extract and transport the holes (positive charges) from the active layer to the electrode [16,17,24]. The performance and stability of solar cells can be increased via the OHTL. To stop the transfer of electrons (negative charges) to the anode, the OHTL functions as an energy barrier [17,24]. The OHTL isolates the moisture in the air, which might deteriorate the active layer, by separating it from the anode [17,24]. OHTLs increase the solar cell's open-circuit voltage while decreasing charge recombination [16,17]. High charge carrier mobility and conductivity are ideal requirements for OHTLs. The HOMO and quasi-Fermi levels of OHTLs should be suitable for reliable hole transfer in a pinhole-free morphology, while OHTLs should also have a high LUMO for efficient electron shielding, thermal, moisture, UV, and chemical resistance, and good morphological contact between the perovskite and the HTL. HTLs should also be created using inexpensive and readily available materials, inexpensive solution-based fabrication techniques that do not harm other solar cell components, and easily reproducible synthesis [14]. Remarkable organic materials that are applied as OHTLs are poly(3,4-ethylenedioxythiophene) (PEDOT), N,N'-bis(3-methylphenyl)-N,N'-diphenylbenzidine (spiro-MeOTAD), poly(3-hexylthiophene) (P3HT), and poly(triaryl amine) (PTAA) (Figure 2a). The energy levels of these materials are presented in Figure 2b.

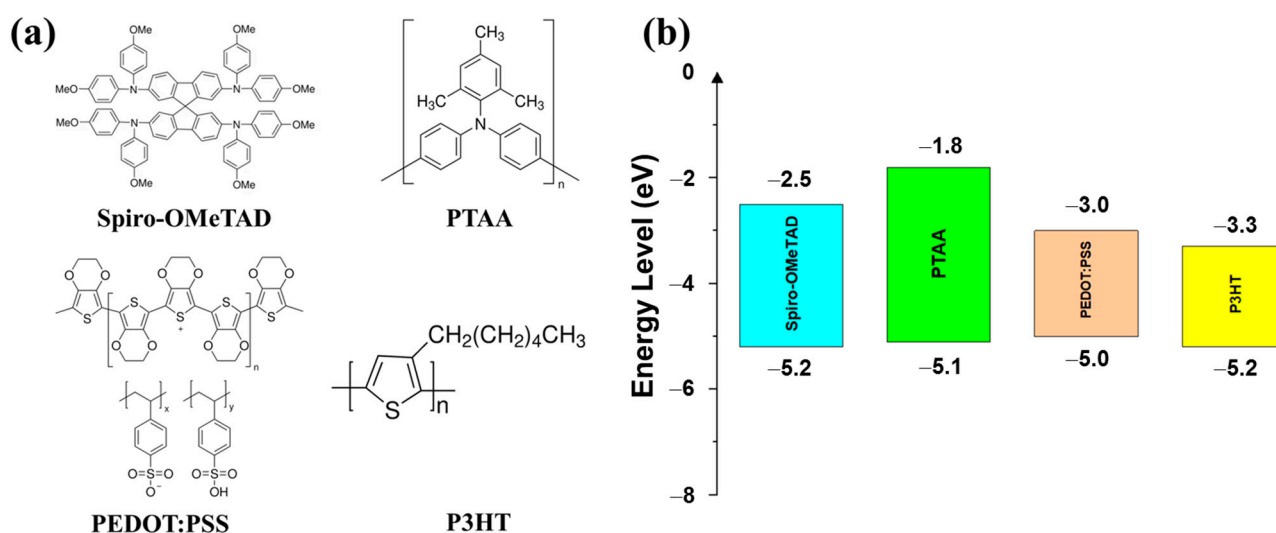


**Figure 2.** (a) Common organic hole transport materials (OHTMs) and (b) their energy levels. Reproduced with permission from ref. [14]. Copyright 2021, Springer Nature.

#### 3.1. Spiro-OMeTAD

The most prevalent HTM in LCSCs is spiro-OMeTAD [14]. Spiro-OMeTAD was used for the first time in PSCs in 2012, displaying an excellent efficiency of 9.7% and significantly better stability than liquid junction PSCs [25]. However, high performance of solar cells can be achieved when spiro-OMeTAD is combined with p-dopants such as lithium bis(trifluoromethanesulfonylimide) (Li-TFSI), 4-*tert* butyloxyridine (tBP), and tris[2-(1*H*-pyrazol-1-yl)-4-*tert*-butylpyridine]cobalt(III)tris(bis(tri-fluoromethylsulfonyl)imide)] [26,27]. By dop-

ing with p-dopants, spiro-OMeTAD is converted to spiro-OMeTAD<sup>+</sup> [28]. Additionally, this is 420 meV deeper in its HOMO, which may result in improved energy alignment at spiro-OMeTAD/perovskite contact [29]. Spiro-OMeTAD has a high hole mobility ( $\mu_h$ ) of  $2 \times 10^{-4} \text{ cm}^2 \cdot \text{V}^{-1} \cdot \text{s}^{-1}$  [26], allowing it to efficiently transport positive charges within the perovskite layer to the electrode and minimize charge recombination losses, thus enhancing device performance. Spiro-OMeTAD possesses suitable energy level alignment, allowing it to selectively transport holes while preventing the transport of electrons. At perovskite contact, spiro-OMeTAD displays a LUMO of  $-1.5 \text{ eV}$  and a HOMO of  $-5.0 \text{ eV}$  (0.1 eV). A number of distinct perovskite conduction bands (CB) are more than 2 eV above the LUMO of spiro-OMeTAD, which suggests strong blocking properties [30]. This guarantees efficient and loss-free extraction of charge carriers from the perovskite layer. Spiro-OMeTAD has shown good chemical and thermal stability, which is important for maintaining the long-term performance of perovskite solar cells. Spiro-OMeTAD is compatible with the deposition techniques commonly used for perovskite fabrication, such as solution processing. On top of the perovskite material, a smooth and homogeneous layer of spiro-OMeTAD can be created by using a suitable solvent, such as chloroform [31,32]. The structure of spiro-OMeTAD allows for efficient hole extraction at the interface between the perovskite absorber layer and the HTM layer, reducing charge recombination and enhancing device efficiency [18]. Lastly, spiro-OMeTAD is commercially available and relatively easy to synthesize, making it accessible for researchers and manufacturers.

Spiro-OMeTAD, despite its popularity as an HTM in PSCs, has several limitations that researchers are actively working to address. Spiro-OMeTAD is remarkable costly at a staggering 29.36 USD per milliliter, and the synthesis of spiro-OMeTAD can be quite intricate, involving multiple steps that necessitate the use of expensive materials, such as palladium (Pd) catalysts [33,34]. Additionally, its commercial availability can lead to higher costs compared to other materials, potentially affecting the scalability of perovskite solar cell manufacturing. Due to exposure to air, moisture, and light, spiro-OMeTAD can deteriorate over time. This can lead to a decrease in device performance and efficiency, particularly in long-term outdoor applications. For example, the dopants Li-TFSI and tBP easily break down spiro-OMeTAD and perovskite films, which makes the PCE less stable over time. Recently, Liu et al. (2023) introduced 1-dodecanethiol (DDT), an alkylthiol additive, in spiro-OMeTAD. This integration made the structure of the HTM more resistant to heat, moisture, and light stress, shortened the time it takes to dope, and reduced the amount of Li-TFSI<sub>2</sub> that builds up at the interfaces. The devices based on spiro-OMeTAD stabilized with DDT exhibited a PCE of 23.1%. The units could maintain 90% of their peak performance for 1,000 h of continuous illumination [35]. The moisture resistance of spiro-OMeTAD-based solar cells can also be enhanced by the replacement of Li-TFSI with more hydrophobic additives such as Zn-TFSI<sub>2</sub>, Mg-TFSI<sub>2</sub>, and Ca-TFSI<sub>2</sub> [36,37]. There are also some efforts to produce spiro-OMeTAD-based PSCs without the use of Li-TFSI. The LiTFSI-free spiro-OMeTAD by Tan et al. (2019) could achieve a PCE of 19.3% (Figure 3) [38]. While spiro-OMeTAD has been successful in achieving suitable energy level alignment for hole transport, it is not a perfect match for all perovskite compositions. Tailoring energy level alignment to different perovskite materials can be a challenge. At elevated temperatures, the performance of spiro-OMeTAD-based devices is decreased due to the significantly lower glass transition temperature of oxidized spiro-OMeTAD<sup>+</sup> [39–41]. In addition, weak contacts at the spiro-OMeTAD/perovskite interface and reinforcement of the film brought on by a buildup of additives at the interface cause poor adhesion [42]. By including a polyethyleneimine (PEI) interlayer between spiro-OMeTAD and perovskite, this restriction can be bypassed [43]. Additionally, under continuous illumination, photodegradation of the chemical interaction between spiro-OMeTAD and Au at the interface is seen [44]. In addition, spiro-OMeTAD is a poor barrier for Au migration into the perovskite [18]. To prevent electrode diffusion and boost stability, a bilayer Cu-Ag electrode has been employed [45]. Spiro-OMeTAD contains heavy metals, which can raise environmental and health concerns. The use of toxic or environmentally unfriendly materials is an ongoing



challenge for sustainable solar cell technologies. Spiro-OMeTAD itself does not absorb light in the visible spectrum, which means it does not contribute to light absorption in the device. This can lead to suboptimal utilization of incident sunlight. In thick perovskite layers, it can be hard for spiro-OMeTAD to pull out charges that are made deep within the perovskite layer. This could cause charges to build up and energy to be lost.

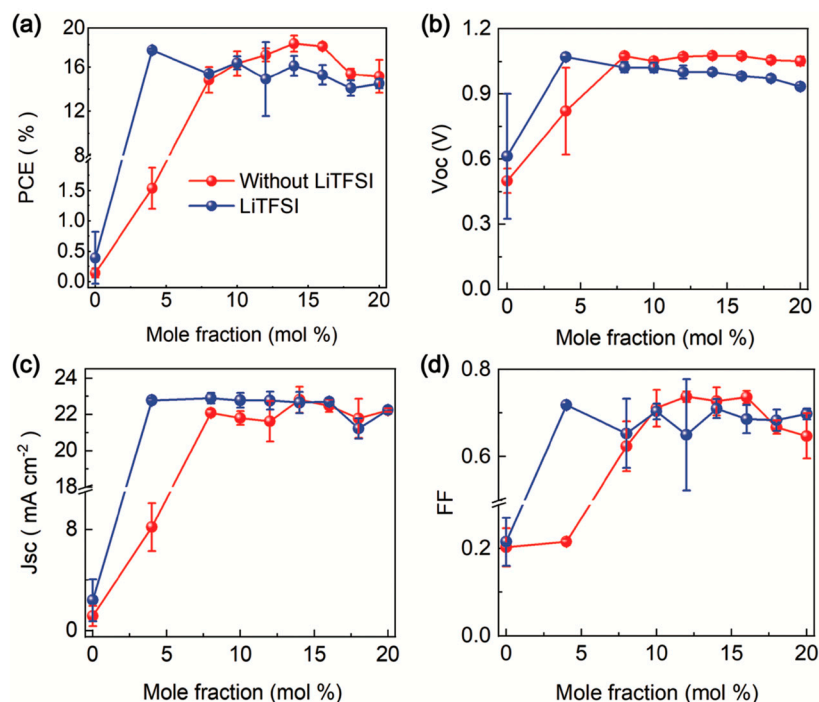


**Figure 3.** Performance of PSCs based on spiro-OMeTAD(TFSI)<sub>2</sub> in the absence (red) and existence (blue) of LiTFSI: (a) PCE, (b) V<sub>OC</sub>, (c) J<sub>SC</sub>, (d) FF. Reprinted with permission from ref. [38] Copyright 2019, Wiley-CH.

Spiro-OMeTAD comprises a spirobifluorene core bound to four bis(methoxyphenyl)amines. The derivatives of bis(methoxyphenyl)amines, with methoxy groups in different positions on the benzene ring (p-OMe, m-OMe, or o-OMe), can significantly alter the physical and chemical properties of spiro-OMeTAD. Jeon et al. investigated how these derivatives of spiro-OMeTAD affect the performance of PSCs [46]. m-OMe tended to withdraw electrons, while p- and o-OMe showed electron-donating behavior; therefore, the PSCs using m-OMe spiro-OMeTAD showed low performance [46]. The investigation showed that p- and o-OMe at a ratio of 2:2 in spiro-OMeTAD showed a significant improvement in PSCs with a PCE of ~16.7% and FF of 77.6%, while only p-OMe spiro-OMeTAD exhibited a PCE of 15% and FF of 71.1%. Other spiro-OMeTAD derivatives could be formed by replacing the spirobifluorene core with cores of pyrene, thiophene, tetraphenylethene, etc., which would provide a different energy configuration for mobility, HOMO, and LUMO levels [47–52]. Saliba et al. (2016) utilized a fluorene–dithiophene (FDT) core substituted with donor groups to create a new hole transport material (HTM) with a high adiabatic oxidation potential of approximately 5.15 eV, surpassing that of spiro-OMeTAD at approximately 4.98 eV. This higher potential indicated increased stability. FDT-based HTM in perovskite solar cells (PSCs) exhibited improved J<sub>SC</sub> and V<sub>OC</sub> when compared to spiro-OMeTAD-based devices, resulting in an impressive PCE of approximately 20.2% and enhanced long-term stability [53]. Zhang et al. (2018) employed spiro[fluorene-9,9'-xanthene] (SFX) as a new core for synthesizing new HTMs, X26 and X36, which exhibited higher conductivity than spiro-OMeTAD by 2–5 times [54]. The X26-based devices showed a high PCE of ~20.2%. Moreover, under controlled humidity of ~20%, the devices could maintain a PCE of 18.8% after 5 months, indicating the highly stability of the new HTMs. Jeong et al. (2022)

successfully fabricated spiro-Naph as an HTM for PSCs, which exhibited an impressive PCE of 24.43% [55]. Moreover, the devices showed excellent stability and thermal endurance at an elevated temperature of 60 °C after 400 h. The improvement came from a significantly high hole mobility of  $\sim 8 \times 10^3 \text{ cm}^2 \text{ V}^{-1} \text{ s}^{-1}$  and the HOMO level of spiro-Naph was closer to the HOMO of perovskite materials; therefore, the transportation of holes was facilitated. In general, the use of different cores leads to the tuning of energy level of the HTM, offering more flexibility in achieving a low energy barrier for efficient hole transport within the solar cell configuration [56]. In addition, improvement in hole mobility is also enhanced with the introduction of more benzene rings with functional groups.

### 3.2. PTAA

Poly[bis(4-phenyl)(2,4,6-trimethylphenyl)amine] (PTAA) has attracted interest as a potential HTM in a variety of optoelectronic devices, including solar cells. PTAA is a type of polymer that is often used as a replacement for other hole transport materials, such as spiro-OMeTAD, due to its favorable electronic properties and ease of processing [57]. PTAA has excellent solubility in a variety of organic solvents and an amorphous, thermally stable shape. Neither the melting phase nor the glass transition were visible in pure PTAA up to 300 °C [58]. When LiTFSI and tBP were used to dope all HTLs, PTAA outperformed a variety of other semiconducting polymers, including spiro-OMeTAD, to achieve an efficiency of 12% in PSCs in 2013 [59,60]. Similar to spiro-OMeTAD, PTAA only functions well in the presence of supplements and causes instability problems [10]. The performance of PSCs with pristine PTAA could reach a PCE of 18.11% [61], while the combination of PTAA and dopants such as Li-TFSI could lead to a PSC with a PCE of 19.7% for 1 cm<sup>2</sup> cells [62]. The optimal doping concentrations for PTAA-based PSCs are, however, roughly four times less than the typical concentrations of tBP and LiTFSI added to spiro-OMeTAD [63]. PTAA can be synthesized using simpler and more scalable methods compared to spiro-OMeTAD, potentially leading to lower production costs. Other hole-conducting polymers did not interact with the perovskite at the interface as strongly as PTAA, which may have improved hole transport [18]. PTAA is considered to be more environmentally friendly than spiro-OMeTAD, which contains heavy metal elements. Although PTAA is still expensive (19.80 USD/mL), its cost is still lower than that of spiro-OMeTAD [33].

While PTAA has shown promise, its hole mobility and charge extraction efficiency can still be lower than those of spiro-OMeTAD in some cases [64]. Greater quality and defect passivation in the perovskite at the interface was partly responsible for PTAA's lower rates of recombination compared to other widely used HTMs [65]. Similar to spiro-OMeTAD, despite the strong thermal durability of pure PTAA, thermal strain does cause perovskite cracks in doped PTAA-based PSCs, leading to a 60% efficiency reduction [66]. PTAA is also sensitive to moisture and is not a reliable barrier to ionic diffusion [18]. Another limitation of PTAA comes from its hydrophobicity, which prevents PTAA film from developing high-quality perovskite [57,67]. Bagheri et al. (2020) overcame this limitation when applying PTAA in the inverted PSC (p-i-n) architecture by preparing the PTAA layer with a quick UV treatment before perovskite was deposited [67]. The PTAA layer's PCE was 19.17% for a 0.09 cm<sup>2</sup> active area due to improvements in the optical characteristics, grain size, and the decrease in recombination centers. The device also kept more than 75% of its initial efficiency after 1400 h of storage under atmospheric conditions with an average relative humidity (RH) of 50% [67]. In other study, Li et al. (2022) modified the surface of PTAA with 4,4',4''-(1-hexyl-1H-dithieno[3',2':3,4:2'',3'':5,6]benzo[1,2-d]imidazole-2,5,8-tryl)tris(N,N-bis(4-methoxyphenyl)aniline) (denoted as M2) [57]. Due to improved PTAA hydrophobicity, M2's presence promoted the development of perovskite film. PTAA/M2 also had greater hole conductivity and mobility compared to pristine PTAA. The application of M2 increased the PCE of inverted PSCs from 18.67% to 20.23% (Figure 4) [57]. Spiro-OMeTAD is commercially available and widely used in research and industry. PTAA might have limited commercial availability. Spiro-OMeTAD has been extensively used as a

benchmark material, and its performance has been well characterized. PTAA is still being evaluated, and its performance might not be as standardized.

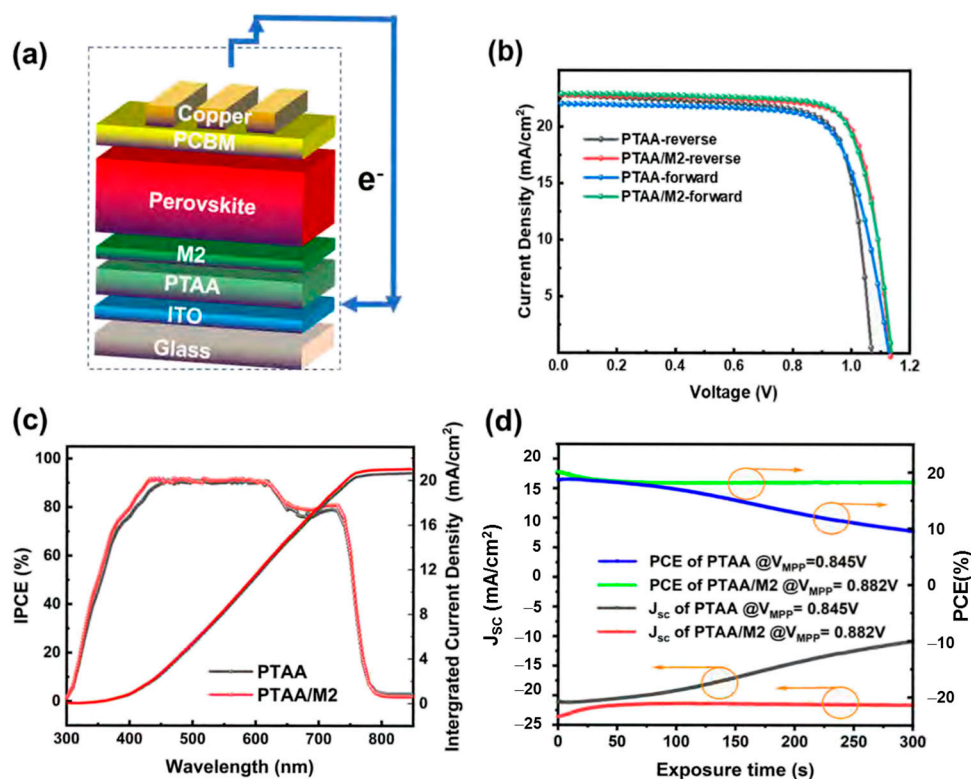


**Figure 4.** (a) The structure of PSCs based on PTAA/M2, (b) current density–voltage characteristics, (c) incident IPCE spectra, (d) stabilized power output, tracked at MPP under AM 1.5G illumination. Reprinted with permission from ref. [57] Copyright 2022, American Chemical Society.

### 3.3. PEDOT:PSS

PEDOT:PSS offers high charge carrier mobility, an adequate band gap, optimal spectrum alignment, and an inexpensive price [14]. Additionally, PEDOT:PSS offers excellent formability and strong transparency in the visible region [68]. PEDOT:PSS has been employed as an HTM in OSCs, facilitating the efficient transport of positive charge carriers (holes) from the photoactive layer to the electrode. While primarily used as a transparent conductive electrode in PSCs, PEDOT:PSS has also been explored as an HTL in certain device architectures. It can effectively transport holes from the perovskite absorber layer to the electrode, contributing to enhanced charge extraction and overall device performance.

However, PEDOT:PSS still has some limitations. PEDOT:PSS contains a polystyrenesulfonate component that is acidic, which can cause the degradation of adjacent layers and impact device stability. Low  $V_{OC}$  ( $<1$  V) is produced as an outcome of the energy gap between PEDOT:PSS ( $-5.12$  eV) and  $\text{CH}_3\text{NH}_3\text{PbI}_3$  ( $-5.4$  eV) perovskites [68]. Achieving optimal energy level alignment between PEDOT:PSS and the active layer can be challenging, affecting charge extraction and recombination dynamics. The existence of the weak ionic conductor PSS limits and impairs charge transfer in PEDOT:PSS [69]. The PSS in PEDOT:PSS can be removed using a simple solvent engineering method (ethylene glycol and methanol). This strategy can increase the PCE of PSC devices to 18.18% [69]. While PEDOT:PSS is an effective conductor, its interfacial properties can impact electron blocking and recombination mechanisms [70]. Inside the PEDOT:PSS layer, poor hole migration can originate from imperfections in the PEDOT:PSS film's microstructure and the gradient of electrical conductivity between the surface and the bulk. This causes an imbalance in carrier charge transfer and the buildup of charge carriers, which finally leads to low FF and large leakage of current [68]. To increase the Fermi level of PEDOT:PSS by up



to 500 meV, Chin et al. (2022) dedoped it using NaOH. Enhanced photoluminescence duration and greater photovoltage of the surface, which resulted in higher  $V_{OC}$ , fill factor, and PCE, were signs that recombination losses were significantly reduced at the dedoped PEDOT:PSS/perovskite interface [70]. PEDOT:PSS is hygroscopic, meaning it can absorb moisture from the environment, which might affect device performance and stability. The moisture sensitivity of PEDOT:PSS can be overcome by the introduction of a crosslinking agent combined with surface treatment [71]. The PEDOT:PSS's crosslinking system converted its naturally water-soluble features into a water-resistance characteristic, preventing water penetration. Additionally, MeOH treatment enhanced PEDOT:PSS's conductivity and decreased its surface roughness by eliminating surface traces [71].

### 3.4. P3HT

Due to its stability, low cost, high hole mobility ( $0.1 \text{ cm}^2 \text{ V}^{-1} \text{ s}^{-1}$ ), and high efficiency, the conjugated polymer poly(3-hexylthiophene) (P3HT) has received extensive study and is utilized as an HTM in organic solar cells (OSCs) [72]. P3HT has a conjugated polymer backbone, which makes it possible for long-range electron delocalization to occur. This results in good charge carrier mobility and efficient charge transport. P3HT can be processed from solution, enabling its incorporation into scalable and cost-effective manufacturing methods, such as spin-coating and printing. P3HT exhibits reasonable electrical conductivity, making it suitable for charge transport within the active layer. Due to its resistance to temperatures in the range of  $-80 \text{ }^\circ\text{C}$  to  $100 \text{ }^\circ\text{C}$ , low oxygen penetration, and extreme hydrophobicity, P3HT is more stable than spiro-OMeTAD [73]. Application of P3HT in mesoporous PSCs on solid substrates produced a PCE of 22.7% when a layer of wide-bandgap halide perovskite was employed on top of a layer of narrow-bandgap perovskite [33].

While P3HT has relatively good hole mobility compared to some other organic materials, it still falls short of the hole mobility exhibited by some inorganic materials. P3HT-based solar cells can experience energy losses due to charge recombination and the formation of non-radiative recombination pathways. Low PCE was caused by poor interaction and significant recombination at the junction between perovskite and P3HT [72]. P3HT has a relatively low absorption coefficient, which can limit its ability to efficiently absorb photons and contributes to photocurrent generation. P3HT-based solar cells can face challenges related to long-term stability under environmental conditions and operational stress. P3HT-based organic solar cells have demonstrated moderate efficiency levels compared to some other organic and inorganic solar cell technologies. A PCE as low as 16% may be attained with pure P3HT as an HTM [74,75]. Different additives like BTCIC-4Cl, copper(I) thiocyanate (CuSCN), n-hexyl trimethyl ammonium bromide (HTAB), gallium (III) acetylacetonate ( $\text{Ga}(\text{acac})_3$ ), and SMe-TATPyr were used to fix problems at the interface between P3HT and perovskite [76,77]. Recently, Xu et al. (2022) used 2-((7-(4-(bis(4-methoxyphenyl)amino)phenyl)-10-(2-(2-ethoxyethoxy)ethyl)-10H-phenoxazin-3-yl)methylene)malononitrile (MDM) as a molecular link for stable and effective PSCs (PCE of 22.87%,  $V_{OC}$  of  $1.15 \pm 0.02$ , and fill factor (FF) of  $75.02 \pm 3.09\%$ ). The triphenylamine group of MDM could create  $\pi$ - $\pi$  stacking with P3HT, creating a charge transfer pathway, whereas the malononitrile group of MDM could bond the perovskite surface. Additionally, MDN greatly reduced recombination and passivated flaws. A total of 92% of the initial PCE of the MDN-P3HT-based PSC device was preserved even after aging for two months at a RH of 75%. Additionally, the PCE remained constant after 500 h of operation under a single sun illumination at the maximum power point (MPP,  $-45 \text{ }^\circ\text{C}$  in  $\text{N}_2$ ) [72].

### 3.5. Other OHTMs

In addition to the OHTMs mentioned, many novel dopant-free OHTMs have also been applied as HTLs for LCSCs. For instance, poly(2,7-carbazole) (PCz) has been used as an HTL. PCz, an aromatic heterocyclic conducting polymer that contains nitrogen, has fast charge mobility, outstanding morphological stability, and great optoelectronic characteristics [78].

Its use in PSCs results in a device PCE of 18.04%. Moreover, it has been demonstrated that PCz functions as a strong barrier and adequately protects the perovskite surface, resulting in highly stable PSC devices [79]. Recently, Wang et al. (2022) drove the self-assembling of carbazole through hydrogen bonding. In comparison to hydrogen bonding-free devices, n-i-p PSC devices based on the hydro-functional HTM showed improved hole extraction reaction, inhibited interfacial charge recombination, decreased hysteresis effect, and significant raises in  $V_{OC}$ , FF, and overall PCE [80]. Organic compounds that are heterocyclic and have rings with carbon and sulfur atoms, like benzothiophene, 1,3-bis(4-(2-ethylhexyl)thiophen-2-yl)-5,7-bis(2-ethylhexyl)benzo[1,2-c:4,5-c']-dithiophene-4,8-dione (BDD), dithieno[3',2':3,4:2'',3'':5,6]benzo[1,3-c][1,2,5]thiadiazole (BTT), random copolymer (RCP) of benzo[1,2-b:4,5-b']dithiophene (BDT), and 2,1,3-benzothiadiazole (BT), have also been applied as HTLs [19,81–83]. He et al. (2023) suggested a solvothermal treatment for benzothiophene to obtain benzothiophene carbon dots (CDs) [81]. The new HOMO value of the obtained material more closely resembled the perovskite valence band. Consequently, these CD-modified PSCs exhibited an acceptable power conversion efficiency (13.22%). The presence of benzothiophene CDs also improved the crystallinity and hydrophobicity of the perovskite film. The increase in hydrophobicity could be related to the generation of a Pb–S bond at the interface between perovskite and benzothiophene CDs [81]. Recently, a PCE of 20.9%,  $V_{OC}$  of 1.14 V,  $J_{SC}$  of 23.4 mA cm<sup>-2</sup>, and FF of 78.9% were achieved by n-i-p PSCs based on BTT, while these values for devices based on BDD were 16.3%, 1.12 V, 23.2 mA cm<sup>-2</sup>, and 62.8%, respectively [19]. A similar HOMO level of -4.9 eV and high hole mobility of over  $5 \times 10^{-4}$  cm<sup>2</sup> V<sup>-1</sup> s<sup>-1</sup> were observed for BDD and BTT [19]. Meanwhile, PSCs with RCPs of BDT and BT as HTMs could reach a PCE of 17.3%. The high mobility and deep HOMO energy level were responsible for the observed PCE. A hydrophobic polymer layer and the avoidance of hygroscopic or deliquescent dopants also increased the long-term PCE. At 75% humidity, PSCs with random copolymers continued to function at their initial PCE for more than 1400 h, but HTM devices with additives had a reduced PCE after 900 h [82]. The remarkable studies that have utilized organic materials as HTMs are summarized in Table 1.

There are some strategies to improve the performance of LCSCs with organic materials as HTLs. Dopant-free organic materials should be considered because they can avoid the use of additives that can increase the instability and toxicity of OHTLs. Some materials have been introduced in the literature, such as D-A- $\pi$ -A-D-type DTP-C6Th, 1,10-phenanthroline (YZ22), DTB-FL, Ni phthalocyanine (NiPc), 2DP-TDB, phenanthrocarbazole 6 (PC6), and Mesh TABT [84–88]. However, even on a lab scale, none of them can actually take the place of doped spiro-OMeTAD [72]. In addition, inorganic materials such as carbon materials (such as carbon nanotubes or graphene), metals (such as aluminum and copper), metal oxides (such as NiO<sub>x</sub> and MoO<sub>x</sub>), or metal compounds (such as CuSCN and CuPc) can be applied to combine the advantages of both inorganic and organic materials [89–93]. PSC efficiency and stability have recently been improved by combining tBP- or Li-TFSI-doped spiro-OMeTAD with fluorinated graphene (FG). The PCE of the PSCs reached 21.92% and further increased to 23.14% when a 2D interfacial layer was installed. FG increased the hydrophobicity of the HTL and enhanced lithium ion reduction in the perovskite layer, in addition to increasing the hole mobility of spiro-OMeTAD. During a 2400 h test in ambient circumstances with 25% RH, the FG-incorporated cell exhibited higher stability, keeping 90% of its initial PCE [93]. However, the introduction of inorganic materials could lead to several negatives, such as high price, low transparency, and possible corrosion [94]. In addition, most inorganic materials are difficult to deposit on top of perovskite [18]. There are also some unique strategies to improve the performance of PSCs using OHTMs as HTLs. For example, Zhang et al. (2023) intertwined single-walled carbon nanotube (SWCNT) electrodes with dopant-free PTAA and applied them in dual roles as the HTL and electrode in PSCs [95]. The PSCs with these dual-role electrodes achieved a better PCE and stability compared to PSCs using LiTFSI-doped spiro-OMeTAD [95].

**Table 1.** Summarization of organic hole transport materials.

HTMs	ABSORBER	V <sub>OC</sub>	J <sub>sc</sub>	FF	PCE	Ref.
<b>Spiro-OMeTAD</b>						
Pristine Spiro-OMeTAD	CH <sub>3</sub> NH <sub>3</sub> PbI <sub>3</sub>	1.0	18.30	73.64	13.48	[43]
Mg-TFSI <sub>2</sub> -doped Spiro-OMeTAD	Triple-cation perovskite (Cs <sub>0.06</sub> FA <sub>0.79</sub> MA <sub>0.15</sub> PbI <sub>2.55</sub> Br <sub>0.75</sub> )	1.091	22.62	76.70	18.93	[36]
Ca-TFSI <sub>2</sub> -doped Spiro-OMeTAD		1.074	22.54	76.50	18.69	
Zn-TFSI <sub>2</sub> -doped Spiro-OMeTAD	Triple-cation perovskite	1.162	23.78	78.80	22.00	[37]
Spiro-OMeTAD(TFSI) <sub>2</sub>	Rb <sub>0.05</sub> Cs <sub>0.05</sub> FA <sub>0.8</sub> MA <sub>0.07</sub> PbBr <sub>0.4</sub> I <sub>2.57</sub>	1.08	23.9	75.00	19.30	[38]
<b>PTAA</b>						
Pristine PTAA	CH <sub>3</sub> NH <sub>3</sub> PbI <sub>3</sub>	1.08	22.44	71.00	18.11	[61]
UV-Treated dopant-free PTAA	Cs <sub>0.05</sub> (MA <sub>0.17</sub> FA <sub>0.83</sub> ) <sub>0.95</sub> Pb(I <sub>0.83</sub> Br <sub>0.17</sub> ) <sub>3</sub>	1.08	22.74	78.00	19.17	[67]
PTAA-MA	Cs <sub>0.05</sub> (MA <sub>0.17</sub> FA <sub>0.83</sub> ) <sub>0.95</sub> Pb(I <sub>0.83</sub> Br <sub>0.17</sub> ) <sub>3</sub>	1.13	22.86	78.16	20.23	[57]
<b>PEDOT:PSS</b>						
Solvent-treated PEDOT:PSS (ethylene glycol + methanol)	MAPbI <sub>3</sub>	1.04	22.21	79.00	18.18	[69]
PEDOT:PSS + PCDSA (MeOH treatment)	MAPbI <sub>3</sub>	0.90	18.88	72.00	13.01	[71]
	PTB7-Th:PC <sub>70</sub> BM	0.72	17.40	59.00	7.71	
	P3HT:PC <sub>60</sub> BM	0.56	9.07	61.00	3.18	
<b>P3HT</b>						
Pristine P3HT	(FAPbI <sub>3</sub> ) <sub>0.95</sub> (MAPbBr <sub>3</sub> ) <sub>0.05</sub> + wide-bandgap halide perovskite (WBH)	1.144	24.92	79.50	22.70	[33]
P3HT-MDN	Cs <sub>0.05</sub> FA <sub>0.85</sub> MA <sub>0.10</sub> Pb(Br <sub>0.03</sub> I <sub>0.97</sub> ) <sub>3</sub>	1.15	24.58	75.02	22.87	[72]
<b>Other OHTMs</b>						
PCz1	Cs <sub>0.08</sub> FA <sub>0.80</sub> MA <sub>0.12</sub> Pb(I <sub>0.88</sub> Br <sub>0.12</sub> ) <sub>3</sub>	1.04	22.41	77.55	18.04	[79]
Hydrogen bonding PCz	Cs <sub>0.05</sub> (MA <sub>0.17</sub> FA <sub>0.83</sub> ) <sub>0.95</sub> Pb(I <sub>0.83</sub> Br <sub>0.17</sub> ) <sub>3</sub>	1.03	22.6	64.7	15.1	[80]
Benzothiophene CDs	MAPbI <sub>3</sub>	1.04	19.57	64.79	13.22	[81]
RCP of BDT and BT	CH <sub>3</sub> NH <sub>3</sub> PbI <sub>3</sub>	1.08	21.9	75	17.3	[82]
BTT	MA <sub>0.7</sub> FA <sub>0.3</sub> PbI <sub>3</sub>	1.14	23.4	78.9	20.9	[19]
BDD		1.23	23.2	62.8	16.3	

## 4. Inorganic Hole Transport Layer (IHTL)

### 4.1. Graphene Oxide and Carbon Derivatives

Graphene oxide (GO) and reduced GO (rGO) have unique optical and electrical properties such as high transparency (94%), high conductivity (0.45 S/cm), easy processing, and an atomic-scale thin layer [96]. GOs have the structure of graphene and contain mixed sp<sup>2</sup> and sp<sup>3</sup> hybridizations of carbon and carbon–oxygen (C–O, C=O, C–OH) covalent bonds, which not only provide a stable structure but also allow tunability of the band gap and work function [97,98]. As reported in the literature, the work functions of GO and rGO are around 4.0–5.0 eV depending on the type of dopant, which is adjustable to fit with the requirements of HTLs in OSCs [99–101]. Li et al. (2010) proposed a solution process to use GO as an HTL in OSCs with P3HT/PCBM as the active material [101]. Using the spin-coating method, very thin layers were obtained with various thicknesses ranging from 2 to 10 nm and a smooth surface with a low roughness of under 1.4 nm, as illustrated in Figure 5a. The method indicated easy processing for a high-quality, thin GO-based HTL. Figure 5b shows the well-matched band gap alignment of GO in the structure of OSCs. Moreover, GO-based HTLs in OSCs showed comparable performance with traditional cells, which promises to be a potential HTM, as shown in Figure 5c. However, GO was pointed out to have low ohmic contact with other layers, which reduces the efficiency of the hole transport process. Thus, GO was reduced to rGO or mixed/doped with other materials to overcome this drawback [102]. Yu et al. (2014) demonstrated the use of GO with PEDOT:PSS

composite, which could enhance the properties of OSCs, and achieved a high PCE of 8.21% in comparison with 7.04% for bare PEDOT:PSS [103]. Meanwhile, Liu et al. (2012) sulfated the GO surface (S-GO) by fuming with sulfuric acid and employed S-GO as an HTL to replace PEDOT:PSS. The S-GO-based devices had a comparable PCE to PEDOT:PSS of ~4.4% [104]. Stratakis et al. (2014) used a laser method to form chlorine-doped GO with a work function of 5.23 eV as an HTL in OSCs, significantly outperforming the reference PEDOT:PSS [105]. Jeon et al. (2014) used a spraying method with a heating process to form a coated GO film on the substrate, resulting in moderately thermally treated rGO as the HTL [106]. Metal/halogen, N dopant, or composite routes for GO/rGO were also investigated to find the best combination of this HTL in OSCs and PSCs, such as Cu, Cl, F, and polyaniline [107–111]. rGO was also used as an HTL in PSCs, which even showed better performance compared to PEDOT:PSS, where the PCE reached ~10.8% [112]. Lou et al. (2017) employed a GO-modified PEDOT:PSS surface, which improved the wettability of the HTL layer; therefore, the PSC performance was improved with a PCE of 15.3% [113].

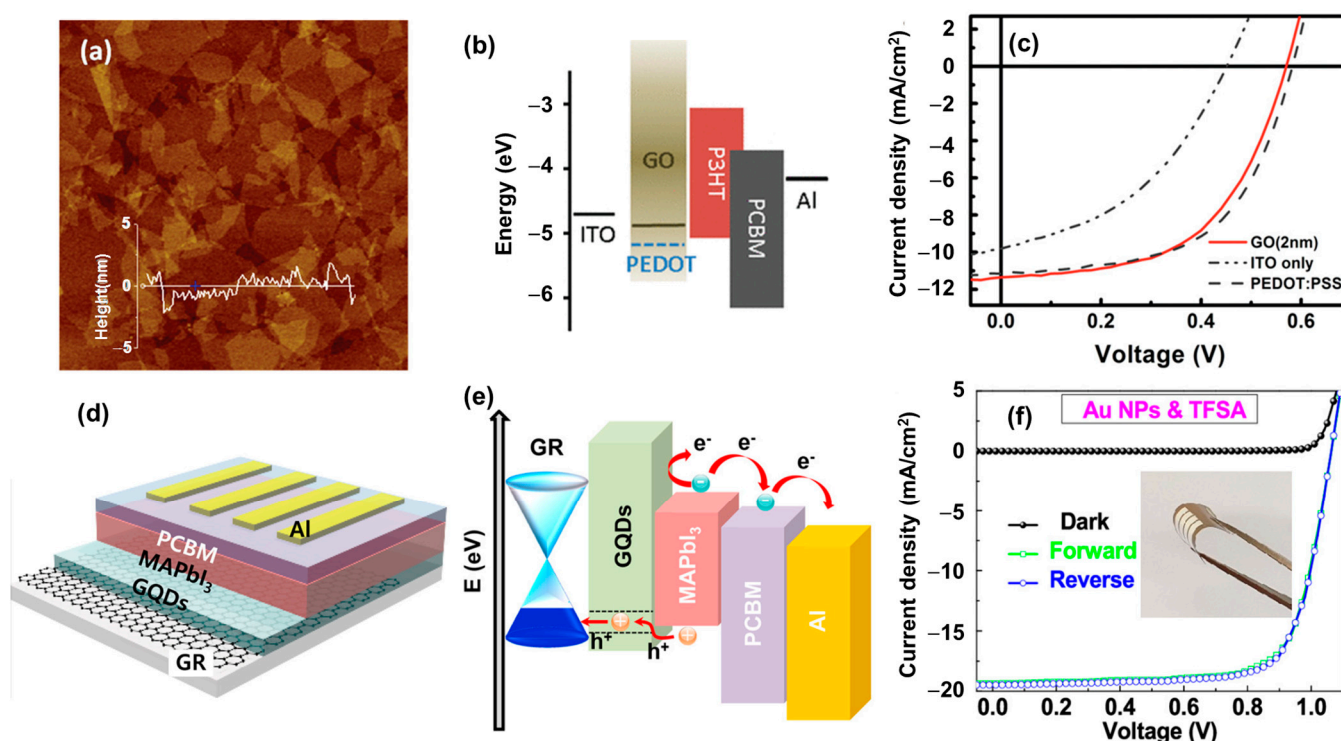


**Figure 5.** (a) Atomic force microscopy image of GO; (b) energy band alignment of GO in OSC structure; (c) J–V curves of GO-, PEDOT:PSS-, and bare ITO-based OSCs. Reproduced with permission from ref. [101] Copyright 2010, American Chemical Society. (d) Structure; (e) energy band alignment; and (f) J–V curves of flexible GQDs and graphene-based MAPbI<sub>3</sub> PSCs. Reprinted with permission from ref. [114] Copyright 2019, American Chemical Society.

In addition, carbon derivatives with a graphene-core structure was also promising to exhibit similar behavior to GO/rGO [114–116]. Graphene quantum dots (GQDs) or carbon dots are well known in optical applications, owing to their fluorescence and electrical properties, which are widely used as biomarkers and light emission materials [117–119]. GQDs are easily fabricated via hydrothermal, microwave-assisted, or solvothermal methods [119–121]. Li et al. (2013) used a one-step acid treatment method to synthesize GQDs from carbon fibers, which were then employed as HTLs in OSCs [122]. The GQD-based devices showed a significant improvement in producibility and lifetime stability, while the PCE was comparable to that of PEDOT:PSS-based devices. Shin et al. (2019) reported employing GQD HTLs in PSCs with Au nanoparticles (NPs), which achieved a PCE of ~15.5% and excellent bending stability of flexible PSCs (retaining 70% PCE after 3000 bending cycles), as shown



in Figure 5d,e [114]. Ali et al. (2023) fabricated vertically aligned CNT thin film as an HTL to protect against direct contact of PEDOT:PSS with the current collector [123]. The CNTs in composition with PEDOT:PSS could improve the stability and increase the conductivity of the HTL. Owing to their high physicochemical properties, low dimensional GO/rGO and carbon derivatives could provide a high mobility, smooth surface with a roughness of a few nm and a huge improvement in stability. However, the low wettability limits their application; therefore, surface modification and functionalization are useful for resolving these issues.

#### 4.2. Metal Oxides

Metal oxide (MO) materials are promising to overcome the challenges of organic HTMs due to their inherent physical/chemical stability and charge conductivity [124]. Especially, transition metal oxide materials have special properties due to their electron structure, which is formed by partially filled d orbitals and the outer shell of valence electrons [125,126]. Nickel oxide ( $\text{NiO}_x$ ) is a p-type direct band gap semiconductor ( $E_g \sim 2.7$  eV) [127]. The valance band of  $\text{NiO}_x$  is well aligned with the HOMO level of many conjugated polymers, and the conduction band is high over the LUMO of the active material [128,129]. Therefore, the band structure of  $\text{NiO}_x$  matches not only the HTL but also the electron-blocking layer (EBL). Due to its high stability,  $\text{NiO}_x$  can be prepared by a variety of methods, such as sol-gel, electrodeposition, oxidation, and spray [128,130–134]. Parthiban et al. (2017) produced  $\text{NiO}_x$  by a solution process, with a valance band of 5.3 eV, which could improve the stability of OSCs and exhibited a comparable PCE to PEDOT:PSS-based devices [135]. Kim fabricated a compact  $\text{NiO}$  film on an FTO electrode, which could improve the PCE from 5.68% to 6.91%, and the use of both  $\text{NiO}$  and PEDOT:PSS could boost the PCE to 7.93%, as shown in Figure 6a–d [136]. In addition,  $\text{NiO}_x$  is commonly used as an HTL in PSCs due to its own properties, low electrode polarization, and suitable surface for growth of the perovskite layer [137]. Liu et al. (2018) employed  $\text{NiO}_x$  as an HTL in methylammonium (MA)-mixed formamidinium (FA) halide (I, Br, Cl) perovskite solar cells, which increased the PCE to 20% [138]. The role of  $\text{NiO}_x$  is not only to be a simple HTL layer but also to enhance the open voltage of PSCs [139].  $\text{NiO}_x$  has been modified by various techniques, such as metal doping (Cu, Li, Mg, Cs, and Zn), surface modification, and the UV-ozone technique, to obtain suitable band alignment with OSC structures [140–146].

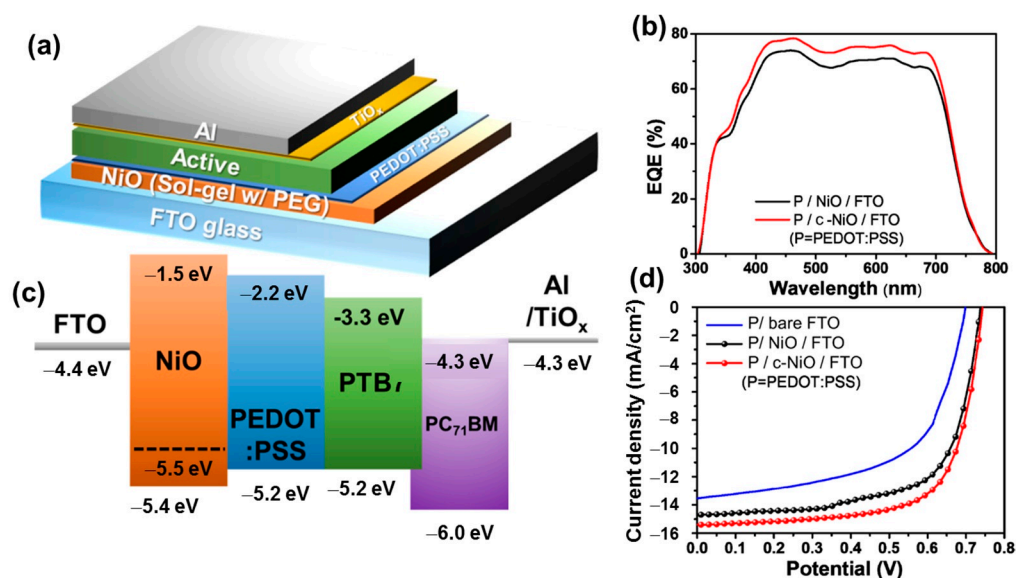


**Figure 6.** (a) Cell structure; (b) external quantum efficiency; (c) band alignment of energy; and (d) J–V curves of NiO/PEDOT:PSS HTL-based OSCs. Reproduced with permission from ref. [136] Copyright 2019, MDPI.

Molybdenum oxide ( $\text{MoO}_x$ ) and tungsten oxide ( $\text{WO}_x$ ) are also commonly used in OSCs.  $\text{MoO}_x$  and  $\text{WO}_x$  are n-type semiconductors with a wide band gap of  $\sim 3.0$  eV, a suitable work function of  $\sim 5.0$  eV, and high surface energy, which would be a potential HTL in OSCs and PSCs [147,148]. A wide band gap allows light to easily pass through. Also, it is easy to make thin films of  $\text{MoO}_x$  and  $\text{WO}_x$  using physical or chemical methods. This means that  $\text{MoO}_x$  and  $\text{WO}_x$  can be used in both normal and inverted structures of OSCs and PSCs. Jasieniak et al. (2012) proposed a solution process to create  $\text{MoO}_x$  thin film using the electrospray ionization method as an HTL in OSCs [149]. The presence of Mo(V) in  $\text{MoO}_x$  revealed that increasing the ratio of  $\text{Mo}^{5+}/\text{Mo}^{6+}$  (from 0.02 to 0.25%) by annealing treatment could improve the performance of OSCs from low to comparable with PEDOT:PSS-based cells. Yang et al. (2018) prepared an n-doped  $\text{MoO}_x$  thin film with a conductivity as high as up to 11 S/cm by introducing a part of Mo(V) to Mo(IV) [150]. The OSC devices with a 10 nm thin film of n-doped  $\text{MoO}_x$  as an HTL showed a high PCE of 11.4%. Modification by the dopant effect introduced a work function of  $\sim 4.9$  eV, which reduced the energy barrier for the extraction of holes from the active material to the current collector and enhanced the performance and stability of OSCs. Liu et al. (2023) reported that the use of  $\text{MoO}_x$  as an HTL could boost the PCE of OSCs to 16.8% and provided excellent air stability over 600 h compared to the PCE of  $\sim 16.4\%$  and the lifetime of 70 h of PEDOT:PSS-based devices at  $85^\circ\text{C}$  [147]. Han et al. (2009) employed  $\text{WO}_3$  thin film as an HTL, which enhanced the performance of OSCs [151]. The  $\text{WO}_3$  amorphous film could reduce the roughness of the thin film to  $\sim 0.88$  nm. Further, the low surface energy of  $\text{WO}_3$  led to the uniform growth of P3HT; therefore, the recombination of charge carriers was reduced. In a similar approach, amorphous  $\text{WO}_x$  was widely used as an HTL in OSC or PSC devices [152–154]. Stubhan reported a low-temperature process to fabricate  $\text{WO}_3$  as an HTL without various treatments, such as oxygen-plasma or annealing treatment. Moreover, Liu et al. (2018) also used the combination of  $\text{WO}_3$  with PEDOT:PSS to reduce the hole transport barrier to the ITO collector [155]. Owing to the high band gap and tunable work function via the dopant or oxygen vacancy,  $\text{WO}_x$  could also be used as an ETL in PCSs or OSCs [156,157].

Besides  $\text{NiO}_x$ ,  $\text{WO}_x$ , and  $\text{MoO}_x$ , metal oxides of Cu, Cr, Co, Ti, and Ir were also used as HTLs, such as  $\text{CuO}_x$ ,  $\text{Cu}_2\text{O}$ , and  $\text{Co}_3\text{O}_4$ , or binary metal oxides such as  $\text{NiCo}_2\text{O}_4$ ,  $\text{CuCrO}_2$ ,  $\text{ZnCo}_2\text{O}_4$ , and  $\text{TiO}_2\text{-IrO}_x$  [158–168]. Yu et al. (2016) demonstrated a solution process of  $\text{CuO}_x$  film for OSCs [164]. The work function of  $\text{CuO}_x$  was tunable via oxidation treatment with  $\text{H}_2\text{O}_2$  or UV-ozone treatment, which increased from 5.06 to 5.45 eV. The  $\text{CuO}_x$  could boost the PCE of OSCs up to 8.68% (10% higher than PEDOT:PSS-based devices). Zhang et al. (2019) used the Mg metal as a dopant in  $\text{CuCrO}_2$  nanoparticles as an HTL in OSCs and PSCs [169]. The presence of Mg not only contributed to decreasing the size of  $\text{CuCrO}_2$ , but also tuned the work function of this material; therefore, the performance of OSCs and PSCs was improved, especially the stability of PSCs (lifetime over 80 h). Liu et al. (2019) used  $\text{Cu}_2\text{O}$  quantum dots by the simple modification method, which could be placed on top of the perovskite layer for inverted PSCs [158]. In general, perovskite material is quite sensitive and can be destroyed by moisture or ionic factors. In this case,  $\text{Cu}_2\text{O}$  quantum dots were not only compact to the perovskite layer but also protected it, achieving a high PCE of 18.9%. Papadas et al. (2018) demonstrated the use of spinel  $\text{NiCo}_2\text{O}_4$  HTM in PSCs [162]. Metal oxides are highly stable materials, benefiting the long-term stability of materials. However, they have drawbacks such as high processing temperatures and low electronic mobility [170]. Therefore, a low processing technique combined with a doping material to increase the electronic mobility is required to employ metal oxides as HTLs.

#### 4.3. Transition Metal Sulfides

Transition metal oxides (TMOs) and transition metal sulfides (TMSs) are also attractive to researchers due to their intrinsic properties. Owing to the higher electron affinity of the S atom compared to the O atom, most TMSs have higher conductivity than TMOs, and the band gap of TMSs is also complex and has a variety of energy band structures [171,172].

Among TMSs, layered structures such as MoS<sub>2</sub>, WS<sub>2</sub>, TiS<sub>2</sub>, and TaS<sub>2</sub> (transition metal dichalcogenides, TMDs) are widely applied in optical/electrical devices due to their superior properties [173–175]. TMDs have a layered structure, with each layer consisting of a transition metal layer (Mo, W, Ti, and Ta) sandwiched between chalcogenide layers (S) and stacked by weak Van der Waals forces to form the bulk structure [176,177]. Therefore, they can easily be fabricated by physical or chemical methods [178,179]. Especially, the energy band structure strongly depends on the number of layers. In the bulk structure, TMDs have a low indirect band gap of ~1.2 eV. When they become single layers, the band gap can be opened to ~2.0 eV as a direct band gap, which not only tunes the band structure but also improves the optical/electrical properties. Moreover, the different stacking of layers leads to different phases, where the 2H phase (hexagonal structure) is semiconductive and the 1T phase (trigonal structure) is metallic [180–183]. Due to the low band gap, TMDs could partially hinder light from passing through; therefore, the use of a very thin layer (increasing transparency) is important [184]. Liang et al. demonstrated MoS<sub>2</sub> nanoflakes as an HTL buffer layer of PSCs (glass/FTO/compact-TiO<sub>2</sub>/mesoporous-TiO<sub>2</sub>/FA<sub>85</sub>MA<sub>15</sub>PbI<sub>85</sub>Br<sub>15</sub>/2D MoS<sub>2</sub>/Spiro-OMeTAD/Au), which exhibited better stability under continuously illumination, as shown in Figure 7a–c [185]. Wang et al. (2018) combined MoS<sub>2</sub> with PEDOT:PSS as a hybrid HTL for PSCs [186]. The MoS<sub>2</sub> nanoflakes improved contact between the composite HTL and the ITO electrode, enhanced the stability of devices up to 28 days, and retained 95% of the initial PCE (18.5%). The pure MoS<sub>2</sub> and WS<sub>2</sub> had work functions that were quite high at ~4.6 eV; therefore, intrinsic TMDs may not effectively transport charge carriers [187–190]. Le et al. (2014) used UV-ozone treatment to partially oxidize MoS<sub>2</sub>/WS<sub>2</sub> to MoS<sub>2</sub>•MoO<sub>x</sub> and WS<sub>2</sub>•WO<sub>x</sub>, reducing the work function to ~5.1 eV, which was compatible with the HOMO level of P3HT:PCBM materials, as shown in Figure 7d,e [188]. The UVO-treated TMDs as HTL devices showed a comparable PCE with PEDOT:PSS-based devices. Xing et al. reported the use of MoS<sub>2</sub> quantum dots with UV-ozone treatment as an HTL in OSCs [191]. The quantum dots provided a low roughness of ~1–2 nm, which benefited the coating process of other layers and reduced the resistance of the contact surface. Additionally, the UV-ozone-treated MoS<sub>2</sub> quantum dots had a work function of ~4.9 eV, which was more suitable to transporting holes from P3HT:PCBM. Adilbekova et al. (2020) employed MoS<sub>2</sub> and WS<sub>2</sub> nanosheets as HTLs in OSCs, which showed a similar PCE to devices based on PEDOT:PSS [192]. The UV-ozone treatment was also performed on WS<sub>2</sub>, TiS<sub>2</sub>, and TaS<sub>2</sub> materials, especially TaS<sub>2</sub>, which had high conducting properties and was also employed as an ETL layer [187–189]. MoS<sub>x</sub> and WS<sub>x</sub> nanodots, or the amorphous structure of MoS<sub>x</sub>•MoO<sub>x</sub> and WS<sub>x</sub>•WO<sub>x</sub>, were also used to make the smooth surface of an HTL by simple solvothermal synthesis [193,194]. This behavior was derived from the partial oxidation of the TMD surface, which not only induced the charge carrier from binding with oxygen but also formed a thin layer of TMD, benefiting the conductivity and stability of the HTL.

TMSs that are not layered materials, such as NiS or CuS, also possess unique properties. CuS and NiS are both p-type semiconductors with work functions ranging from 4.9 to 5.1 eV, which are promising for transporting holes to current collectors [195]. Rao et al. (2016) demonstrated a simple solution process to obtain CuS NPs, which could be a highly stable HTL in PSCs [195]. The CuS thin layer was uniformly coated on the ITO/glass substrate and did not affect the transparency of this substrate. Moreover, the CuS surface was also compact for growth of the active material, lessening the barrier to carrier injection at the interface and improving the performance of PSCs. Li et al. (2020) described the procedure for a room-temperature solution to make p-type CuS<sub>x</sub> thin film as a stable HTL [196]. Tirado et al. (2019) revealed that p-type CuS had a metallic character in the valence band under light irradiation, benefiting the transport of holes and effectively blocking electrons. Thus, it could be used to replace an expensive ETL layer such as spiro-OMeTAD [197]. CuS could also be combined with GO or modified in various compositions, such as CuSCN, Cu<sub>2</sub>CdSnS<sub>4</sub>, and Cu<sub>2</sub>SnS<sub>3</sub>, to improve the hole transport characteristics, surface engineering, and compactness of other kinds of active materials [198–201]. While

CuS has a low band gap of  $\sim 1.5$  eV, NiS possesses a wide range of band gaps from 1.9 to 2.4 eV, depending on the synthesis conditions and capping agents [202,203]. Recently, Hilal et al. (2019) reported the use of NiS nanoflowers as an HTL for OSCs [204]. NiS nanoflowers possess a work function of 5.04 eV, which is reasonable for an HTL layer. Pitchaiya et al. (2018) used NiS-carbon composites as an HTL in PSCs and showed a PCE of 5.2% [205]. However, the transparency of NiS ( $\sim 70\%$ ) is still an obstacle to this HTL [204]. The benefits of metal sulfide materials are their high charge carrier properties, and the S atom is compactable with both inorganic and organic active materials; therefore, they are widely applied in OSCs and PSCs. Owing to their high electronic conductivity and low band gap energy, TMDs are used in inverted structures. However, adjusting the material thickness and UV-ozone treatment could modify their surface and work function to match designated structures in conventional cells. The 1T phase of TMDs is a promising HTL; however, it can gradually transfer back to the 2H phase while suffering a high working temperature. Non-layered TMSs are more stable and can be used as HTLs; however, due to their low transparency, they are generally used as a doping material or thin support layer with another HTL [206].

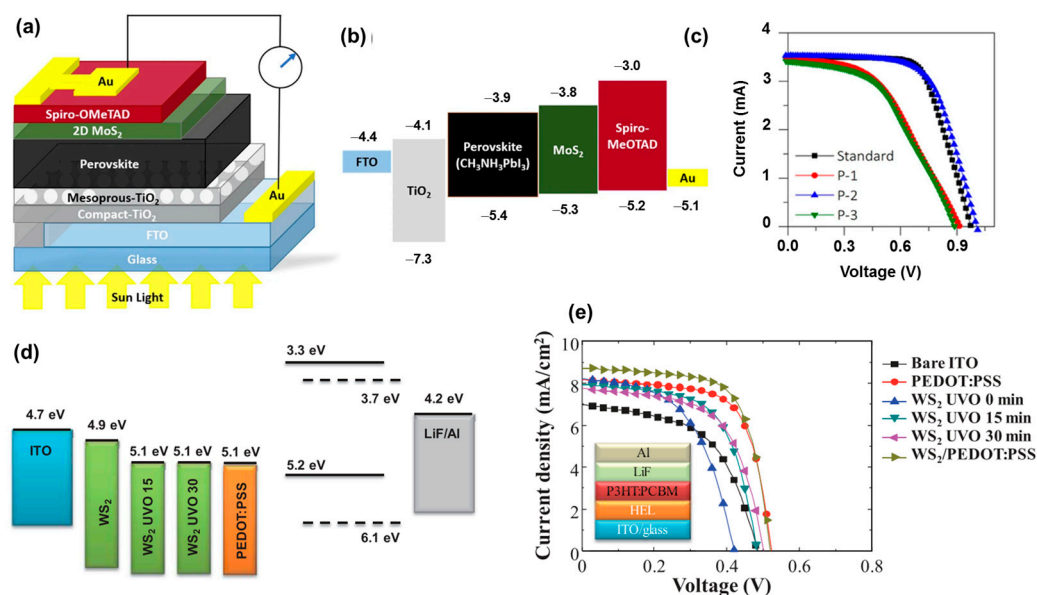


**Figure 7.** (a) Scheme of PSCs based on 2D MoS<sub>2</sub>; (b) energy band alignment of different layers in PSC; (c) J–V curves of devices with different treatments P1, P2, and P3, corresponding with MoS<sub>2</sub> on perovskite without annealing, annealing MoS<sub>2</sub> on pre-annealed perovskite, and annealing MoS<sub>2</sub> on perovskite without annealing, respectively. Reproduced with permission from ref. [185] Copyright 2020, Springer Nature. (d) Energy band alignment work function of WS<sub>2</sub> with/without UV treatment and PEDOT:PSS in OSCs; and (e) J–V curves of devices based on WS<sub>2</sub>-UVO and PEDOT:PSS as HTLs. Reprinted with permission from ref. [188] Copyright 2014, Wiley–CH.

#### 4.4. Organometallic Materials

Recent research on organometallic materials (OMs) has shown the interestingness of organic and metallic properties in a composition. OMs are believed to solve the drawbacks of organic materials, such as low-charge carriers and poor stability, and the drawbacks of inorganic materials, achieving compatibility through surface engineering [34,94,207]. Recently, metal phthalocyanines (MPcs) have received significant attention as OMs for HTLs of PSCs [208]. MPcs have a novel structure with a centered metal atom, which can be easily obtained by a simple reaction of a phthanonitrile-based material with metal salts such as a metal chloride or acetate. MPcs have unique properties, such as a low band gap, high physical/chemical stability, and high carrier mobility [208–211]. Guo et al. (2017) synthesized ZnPc and CuPc and proposed their use as HTMs in PSCs [208]. ZnPc-based



devices achieved high stability after over one month with a comparable open voltage of  $\sim 1.071$  V to Spiro-OMeTAD at 1.107 V. The PCE of devices based on MPc was  $\sim 14.4\%$ , which was still lower than that of Spiro-OMeTAD-based devices (18.9%), but significant improvements in stability and cost-effectiveness would lead this material to becoming a potential HTL, which is also an EBL in PSCs. Using a similar approach, Ni, Zn, and Co metals were also synthesized as MPc materials. Cheng et al. (2017) proposed the use of NiPc and  $V_2O_5$  as a comparative HTL to Spiro-OMeTAD, achieving a PCE of up to 17.6% compared to 18.2%, respectively [212]. In addition, metal porphyrins of Cu and Zn are also promising HTMs, as shown in Figure 8 [213]. CuP and ZnP showed suitable band alignment. Especially, ZnP-based PSCs exhibited a high PCE of 17.78%, which was comparable to that of bare Spiro-OMeTAD-based PSCs (18.59%). Cao et al. (2018) investigated Co(II) and Co(III) porphyrin (CoP) compounds that could boost the PCE of PSCs to 19.6% [214]. Owing to their intrinsic high hole mobility, OMs are generally used as non-doped HTLs [207]. However, their strong absorption limits their use in conventional structures [94]. The use of organometallic materials and inorganic materials as HTLs provides a huge source for building solar cells that effectively convert light into electricity. However, there is still a gap from the experimental to the practical for which detailed factors should be optimized, such as the thickness, surface engineering, structure, cover of the cell, etc. Figure 9 shows some common HTL materials used in PSCs, including MO, MS, and MPc materials. Table 2 also provides a summary of the performance of solar cells employing inorganic and organometallic materials as HTLs, corresponding with the active materials used.

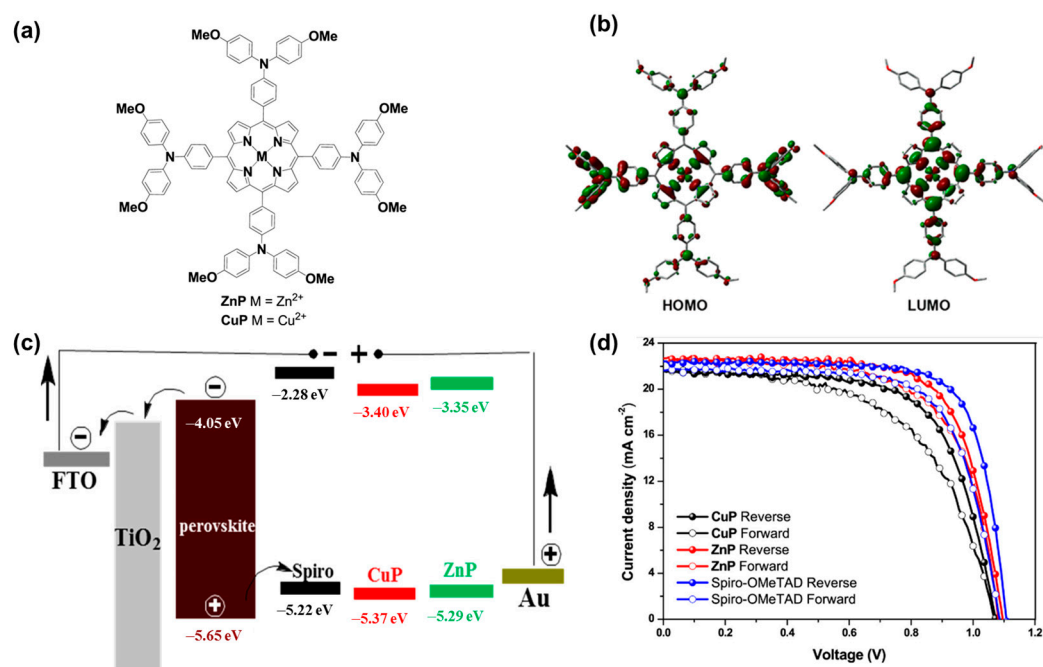


**Figure 8.** (a) Chemical structures of ZnP and CuP with (b) their frontier orbitals; (c) energy band alignment of perovskite and HTLs; and (d) J–V curves measured in reverse and forward voltage scans of CuP, ZnP, and Spiro-OMeTAD-based HTL PSC devices. Reproduced with permission from ref. [213] Copyright 2017, American Chemical Society.

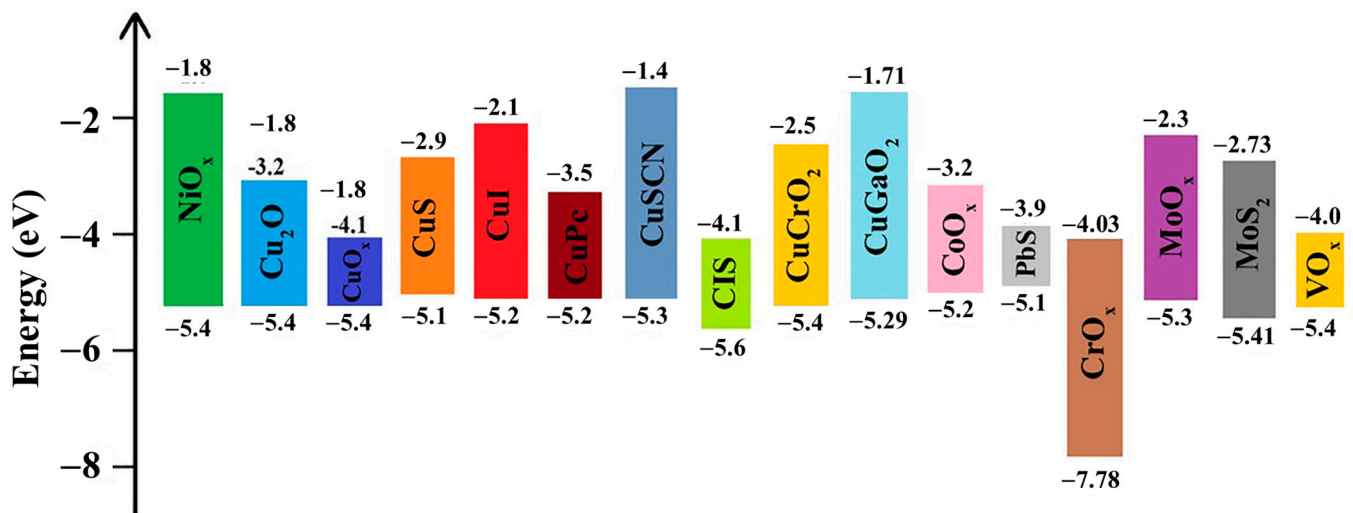


**Figure 9.** Energy level diagrams for commonly used inorganic HTLs in PSCs. Reproduced with permission from ref. [207] Copyright 2021, Wiley-CH.

**Table 2.** Summarization of inorganic and organometallic hole transport materials.

HTM	ABSORBER	V <sub>OC</sub>	J <sub>SC</sub>	FF	PCE	Ref.
<b>GO- and carbon derivative-based HTLs</b>						
GO	P3HT:PC <sub>61</sub> BM	0.57	11.40	54.30	3.50	[101]
PEDOT:PSS/GO	PTB7:PC <sub>71</sub> BM	0.76	16.42	65.80	8.21	[103]
PEDOT:PSS/GO	PCDTBT:PC <sub>71</sub> BM	0.82	10.44	50.00	4.28	[102]
S-GO	P3HT:PC <sub>61</sub> BM	0.61	10.15	71.00	4.37	[104]
CL-GO	PCDTBT:PC <sub>71</sub> BM	0.88	13.65	54.70	6.56	[105]
rGO	P3HT:PC <sub>61</sub> BM	0.58	9.87	65.00	3.71	[106]
N-GO/SnO <sub>2</sub>	Rb-doped-FA-MA-Br-mixed perovskite	1.17	18.87	74.93	16.54	[108]
Cu@RGO	MAPbI <sub>3</sub>	0.97	19.20	69.80	13.23	[109]
F5-GO/PEDOT:PSS	PTB7:PC <sub>71</sub> BM	0.78	15.31	63.00	7.52	[110]
F-rGO	PTB7:Th:PC <sub>71</sub> BM	0.78	16.89	64.80	8.6	[111]
GQDs	Dr3TBDT:PC <sub>71</sub> BM	0.92	11.36	65.20	6.82	[122]
CNT/PEDOT:PSS	P3HT:PC <sub>61</sub> BM	0.55	11.58	58.00	3.69	[123]
O-MWCNTs	Cs-FA-MAPbIBr	0.99	21.96	41.09	8.99	[215]
<b>Metal oxide HTLs</b>						
NiO	PDTG-TPD:PC <sub>71</sub> BM	0.82	13.90	68.40	7.82	[128]
NiO	MAPbI	0.98	21.10	78.00	16.1	[130]
NiO	CsFA-MA-Pb-I-Br	1.02	21.00	85.00	16.7	[131]
Cu doped NiO	MAPbI	1.10	21.73	75.30	18.02	[132]
NiMgO <sub>x</sub>	MAPbI	1.07	21.30	79.00	18.20	[133]
NiO <sub>x</sub>	FA-MA-Pb-I-Cl	1.12	23.70	76.00	20.20	[138]

Table 2. Cont.

HTM	ABSORBER	V <sub>oc</sub>	J <sub>sc</sub>	FF	PCE	Ref.
<b>Metal oxide HTLs</b>						
NiO	AVA-MAPI	0.83	20.90	65.50	10.91	[134]
S-NiO <sub>x</sub>	RP(BDT-PDBT):PC <sub>71</sub> BM	0.71	9.85	63.00	4.45	[135]
MoO <sub>x</sub>	PM6:Y6:PC <sub>71</sub> BM	0.84	26.71	74.22	17.21	[147]
MoO <sub>x</sub>	PB3T2:IT-M	0.96	16.20	68.00	10.50	[150]
s-MoO <sub>x</sub>	P3HT:PC <sub>61</sub> BM	0.59	9.50	68.00	3.80	[149]
WO <sub>3</sub>	P3HT:PC <sub>71</sub> BM	0.61	12.80	60.40	4.80	[216]
WO <sub>x</sub> -PEDOT:PSS	MAPbI <sub>3</sub>	0.97	20.76	70.90	14.30	[155]
Ti <sub>3</sub> C <sub>2</sub> T <sub>x</sub> /WO <sub>3</sub> /PEDOT:PSS	MAPbI <sub>3</sub>	0.90	22.47	60.02	12.26	[153]
O-CuO <sub>x</sub>	PTB7:PC <sub>71</sub> BM	0.74	16.44	71.00	8.52	[164]
<b>Metal sulfide HTLs</b>						
MoS <sub>2</sub>	MAPbI <sub>3</sub>	0.95	20.70	72.30	14.2	[186]
O-MoS <sub>2</sub> QDs	PTB7:Th:PC <sub>71</sub> BM	0.79	16.90	65.00	8.66	[191]
MoS <sub>2</sub> Ns		0.63	12.50	53.20	4.18	
MoS <sub>2</sub>	PBDB-T-2F:Y6:PC <sub>71</sub> BM	0.81	25.30	71.00	14.9	[192]
WS <sub>2</sub>		0.83	26.00	72.00	15.6	
CuS	MAPbI <sub>3</sub>	1.02	22.30	71.20	16.2	[195]
Cu <sub>x</sub> S-GO	TiO <sub>2</sub> /CuInS <sub>2</sub>	0.60	16.06	62.90	6.07	[198]
Cu <sub>2</sub> SnS <sub>3</sub>	FAPbI <sub>3</sub>	1.04	24.14	64.92	16.33	[201]
<b>Organometallic HTLs</b>						
Cop	CsFAMAPbI <sub>3</sub> Br	1.13	23.62	76.66	20.47	[214]
Ni-Pc	FAPbI <sub>3</sub> @MAPbBr <sub>3</sub>	0.895	18.50	63.80	10.6	[212]
Ni-Pc/V <sub>2</sub> O <sub>5</sub>		1.08	23.10	73.40	18.3	
Zn-Pc	MAPbI <sub>3</sub> Br	1.02	22.36	71.43	16.23	[211]
CuPc	FAPbI <sub>3</sub> @MAPbBr <sub>3</sub>	1.07	20.52	66.30	16.36	[213]
ZnPc		~1.10	21.75	71.30	17.78	

## 5. Conclusions and Outlook

In summary, LCSCs such as OSCs, PSCs, and DSSCs have been roughly developed and have reached significant improvements, achieving a PCE of over 24% or even higher with a tandem structure (a combination of 2–3 cells with different ranges of active light into a cell) or light concentrator facilities [217–221]. In order to obtain highly stable devices, the HTL layer has been fabulously investigated with a tremendous variety of materials, from inorganic to organic to organometallic compounds. In general, in comparison with IHTMs, OHTMs have better compatibility with organic active layer materials, which can decrease interfacial errors and increase charge transfer performance [14,17]. OHTMs also have lower costs and easier processability, which can enable large-scale fabrication of solar cells using methods such as printing or coating [14,17,81]. OHTMs have higher transparency and flexibility, which can enable the development of transparent and flexible solar cells for various applications [14,17,81]. In contrast, IHTMs still have higher stability under environmental conditions, such as heat, humidity, or oxygen. IHTMs have higher conductivity and lower resistance than OHTMs, which can improve the charge transport efficiency and decrease the series resistance of solar cells. IHTMs have a wider band gap than organic materials, which can improve the light-harvesting ability of solar cells. Lastly, IHTMs can be produced with simple methods, while OHTMs need multi-step synthesis [14]. The com-

bination of these materials with organic materials balances their properties, in which the high performance of the OHTL and the stability of inorganic materials can be established from their compositions, such as GO/PEDOT:PSS, NiO<sub>x</sub>/PEDOT:PSS, or NiPc-doped spiro-OMeTAD [113,136,212]. Sulfur-based or organometallic materials show a low polarization surface that is easily compacted with the growth of perovskite, improving the performance of PSCs [196,214]. Even though many achievements have been recorded, practical application of these materials is still not well established due to the cost-effectiveness of the processing method, and optimizations need to be investigated. The variable wettability of different HTLs affects the morphology, contact angle, and stability [222]. The rough surfaces and surfaces with pinholes act as defects that trap charge carriers, thereby reducing the PCE. Some materials have high wettability and low contact angles, such as PTAA, spiro-OMeTAD, and PEDOT:PSS; however, surface treatment is also needed to obtain a high-quality surface. Meanwhile, P3HT wettability depends on its formulation and surface treatment. Intrinsic rGO or TMS exhibit high hydrophobicity and functionalization can help reduce the contact angle with another surface, reducing traps and improving the efficiency of the charge transfer process. Meanwhile the wettability of MO depends much on its structure. In general, UV-O treatment greatly helps the surface of inorganic HTLs. In addition, some techniques can be applied to inorganic HTLs, such as modifying thin casting films using the spray method, static/dynamic spin-coating method, using ionic liquids, or incorporating organic molecules as additives [223–226]. Recently, organometallic materials have become promising to replace traditional HTLs with lower costs and high performance. Therefore, there is still a lot of room for studying new materials or optimizing/combining the layer-by-layer structure. Hence, tandem cells are also promising to overcome the light absorption efficiency issues; therefore, the selection of different HTLs for each top/bottom cell needs to be performed. We believe this overview of HTLs could contribute to having a full, bright picture of flexible solar cells in the future.

**Author Contributions:** V.K.H.B.: Conceptualization, visualization, writing, review, and editing. T.P.N.: Conceptualization, writing, review, and editing. All authors have read and agreed to the published version of the manuscript.

**Funding:** This research received no external funding.

**Institutional Review Board Statement:** Not applicable.

**Data Availability Statement:** Not applicable.

**Conflicts of Interest:** The authors declare no conflict of interest.

## References

1. Kojima, A.; Teshima, K.; Shirai, Y.; Miyasaka, T. Organometal Halide Perovskites as Visible-Light Sensitizers for Photovoltaic Cells. *J. Am. Chem. Soc.* **2009**, *131*, 6050–6051. [[CrossRef](#)]
2. Lee, M.M.; Teuscher, J.; Miyasaka, T.; Murakami, T.N.; Snaith, H.J. Efficient Hybrid Solar Cells Based on Meso-Superstructured Organometal Halide Perovskites. *Science* **2012**, *338*, 643–647. [[CrossRef](#)] [[PubMed](#)]
3. Min, H.; Lee, D.Y.; Kim, J.; Kim, G.; Lee, K.S.; Kim, J.; Paik, M.J.; Kim, Y.K.; Kim, K.S.; Kim, M.G.; et al. Perovskite solar cells with atomically coherent interlayers on SnO<sub>2</sub> electrodes. *Nature* **2021**, *598*, 444–450. [[CrossRef](#)] [[PubMed](#)]
4. Hou, Y.; Aydin, E.; De Bastiani, M.; Xiao, C.; Isikgor, F.H.; Xue, D.-J.; Chen, B.; Chen, H.; Bahrami, B.; Chowdhury, A.H.; et al. Efficient tandem solar cells with solution-processed perovskite on textured crystalline silicon. *Science* **2020**, *367*, 1135–1140. [[CrossRef](#)] [[PubMed](#)]
5. Green, M.A.; Ho-Baillie, A.; Snaith, H.J. The emergence of perovskite solar cells. *Nat. Photonics* **2014**, *8*, 506–514. [[CrossRef](#)]
6. Szabó, G.; Park, N.-G.; De Angelis, F.; Kamat, P.V. Are Perovskite Solar Cells Reaching the Efficiency and Voltage Limits? *ACS Energy Lett.* **2023**, *8*, 3829–3831. [[CrossRef](#)]
7. Ikram, M.; Malik, R.; Raees, R.; Imran, M.; Wang, F.; Ali, S.; Khan, M.; Khan, Q.; Maqbool, M. Recent advancements and future insight of lead-free non-toxic perovskite solar cells for sustainable and clean energy production: A review. *Sustain. Energy Technol. Assess.* **2022**, *53*, 102433. [[CrossRef](#)]
8. Sharma, D.; Mehra, R.; Raj, B. Comparative study of hole transporting layers commonly used in high-efficiency perovskite solar cells. *J. Mater. Sci.* **2022**, *57*, 21172–21191. [[CrossRef](#)]
9. Brabec, C.J.; Gowrisanker, S.; Halls, J.J.M.; Laird, D.; Jia, S.; Williams, S.P. Polymer–Fullerene Bulk-Heterojunction Solar Cells. *Adv. Mater.* **2010**, *22*, 3839–3856. [[CrossRef](#)]



10. Krebs, F.C. Fabrication and processing of polymer solar cells: A review of printing and coating techniques. *Sol. Energy Mater. Sol. Cells* **2009**, *93*, 394–412. [[CrossRef](#)]
11. Dou, L.; You, J.; Hong, Z.; Xu, Z.; Li, G.; Street, R.A.; Yang, Y. 25th Anniversary Article: A Decade of Organic/Polymeric Photovoltaic Research. *Adv. Mater.* **2013**, *25*, 6642–6671. [[CrossRef](#)] [[PubMed](#)]
12. Sharma, K.; Sharma, V.; Sharma, S.S. Dye-Sensitized Solar Cells: Fundamentals and Current Status. *Nanoscale Res. Lett.* **2018**, *13*, 381. [[CrossRef](#)] [[PubMed](#)]
13. Kokkonen, M.; Talebi, P.; Zhou, J.; Asgari, S.; Soomro, S.A.; Elsehrawy, F.; Halme, J.; Ahmad, S.; Hagfeldt, A.; Hashmi, S.G. Advanced research trends in dye-sensitized solar cells. *J. Mater. Chem. A* **2021**, *9*, 10527–10545. [[CrossRef](#)]
14. Li, S.; Cao, Y.-L.; Li, W.-H.; Bo, Z.-S. A brief review of hole transporting materials commonly used in perovskite solar cells. *Rare Met.* **2021**, *40*, 2712–2729. [[CrossRef](#)]
15. Liao, K.; Li, C.; Xie, L.; Yuan, Y.; Wang, S.; Cao, Z.; Ding, L.; Hao, F. Hot-Casting Large-Grain Perovskite Film for Efficient Solar Cells: Film Formation and Device Performance. *Nanomicro Lett.* **2020**, *12*, 156. [[CrossRef](#)]
16. Anrango-Camacho, C.; Pavón-Ipiales, K.; Frontana-Uribe, B.A.; Palma-Cando, A. Recent Advances in Hole-Transporting Layers for Organic Solar Cells. *Nanomaterials* **2022**, *12*, 443. [[CrossRef](#)] [[PubMed](#)]
17. Xu, H.; Yuan, F.; Zhou, D.; Liao, X.; Chen, L.; Chen, Y. Hole transport layers for organic solar cells: Recent progress and prospects. *J. Mater. Chem. A* **2020**, *8*, 11478–11492. [[CrossRef](#)]
18. Rombach, F.M.; Haque, S.A.; Macdonald, T.J. Lessons learned from spiro-OMeTAD and PTAA in perovskite solar cells. *Energy Environ. Sci.* **2021**, *14*, 5161–5190. [[CrossRef](#)]
19. Yin, X.; Song, J.; Hu, L.; Jin, Y.; Lu, L.; Su, Z.; Li, Z. Novel dopant-free hole transport materials enabling 20.9% efficiency in perovskite solar cells. *Chem. Commun.* **2022**, *58*, 7940–7943. [[CrossRef](#)]
20. Krishna, A.; Grimsdale, A.C. Hole transporting materials for mesoscopic perovskite solar cells—Towards a rational design? *J. Mater. Chem. A* **2017**, *5*, 16446–16466. [[CrossRef](#)]
21. Park, G.; Kim, D.; Kim, G.; Jeong, U. High-Performance Indium–Tin Oxide (ITO) Electrode Enabled by a Counteranion-Free Metal–Polymer Complex. *ACS Nanosci. Au* **2022**, *2*, 527–538. [[CrossRef](#)] [[PubMed](#)]
22. Shrotriya, V.; Li, G.; Yao, Y.; Moriarty, T.; Emery, K.; Yang, Y. Accurate Measurement and Characterization of Organic Solar Cells. *Adv. Funct. Mater.* **2006**, *16*, 2016–2023. [[CrossRef](#)]
23. Sun, L.; Fukuda, K.; Someya, T. Recent progress in solution-processed flexible organic photovoltaics. *Npj Flex. Electron.* **2022**, *6*, 89. [[CrossRef](#)]
24. Nowsherwan, G.A.; Samad, A.; Iqbal, M.A.; Mushtaq, T.; Hussain, A.; Malik, M.; Haider, S.; Pham, P.V.; Choi, J.R. Performance Analysis and Optimization of a PBDB-T:ITIC Based Organic Solar Cell Using Graphene Oxide as the Hole Transport Layer. *Nanomaterials* **2022**, *12*, 1767. [[CrossRef](#)] [[PubMed](#)]
25. Kim, H.-S.; Lee, C.-R.; Im, J.-H.; Lee, K.-B.; Moehl, T.; Marchioro, A.; Moon, S.-J.; Humphry-Baker, R.; Yum, J.-H.; Moser, J.E.; et al. Lead Iodide Perovskite Sensitized All-Solid-State Submicron Thin Film Mesoscopic Solar Cell with Efficiency Exceeding 9%. *Sci. Rep.* **2012**, *2*, 591. [[CrossRef](#)] [[PubMed](#)]
26. Hawash, Z.; Ono, L.K.; Qi, Y. Recent Advances in Spiro-MeOTAD Hole Transport Material and Its Applications in Organic–Inorganic Halide Perovskite Solar Cells. *Adv. Mater. Interfaces* **2018**, *5*, 1700623. [[CrossRef](#)]
27. Schloemer, T.H.; Christians, J.A.; Luther, J.M.; Sellinger, A. Doping strategies for small molecule organic hole-transport materials: Impacts on perovskite solar cell performance and stability. *Chem. Sci.* **2019**, *10*, 1904–1935. [[CrossRef](#)]
28. Cappel, U.B.; Daeneke, T.; Bach, U. Oxygen-Induced Doping of Spiro-MeOTAD in Solid-State Dye-Sensitized Solar Cells and Its Impact on Device Performance. *Nano Lett.* **2012**, *12*, 4925–4931. [[CrossRef](#)]
29. Fantacci, S.; De Angelis, F.; Nazeeruddin, M.K.; Grätzel, M. Electronic and Optical Properties of the Spiro-MeOTAD Hole Conductor in Its Neutral and Oxidized Forms: A DFT/TDDFT Investigation. *J. Phys. Chem. C* **2011**, *115*, 23126–23133. [[CrossRef](#)]
30. Schulz, P.; Edri, E.; Kirmayer, S.; Hodes, G.; Cahen, D.; Kahn, A. Interface energetics in organo-metal halide perovskite-based photovoltaic cells. *Energy Environ. Sci.* **2014**, *7*, 1377–1381. [[CrossRef](#)]
31. Ono, L.K.; Raga, S.R.; Remeika, M.; Winchester, A.J.; Gabe, A.; Qi, Y. Pinhole-free hole transport layers significantly improve the stability of MAPbI<sub>3</sub>-based perovskite solar cells under operating conditions. *J. Mater. Chem. A* **2015**, *3*, 15451–15456. [[CrossRef](#)]
32. Juarez-Perez, E.J.; Leyden, M.R.; Wang, S.; Ono, L.K.; Hawash, Z.; Qi, Y. Role of the Dopants on the Morphological and Transport Properties of Spiro-MeOTAD Hole Transport Layer. *Chem. Mater.* **2016**, *28*, 5702–5709. [[CrossRef](#)]
33. Jung, E.H.; Jeon, N.J.; Park, E.Y.; Moon, C.S.; Shin, T.J.; Yang, T.-Y.; Noh, J.H.; Seo, J. Efficient, stable and scalable perovskite solar cells using poly(3-hexylthiophene). *Nature* **2019**, *567*, 511–515. [[CrossRef](#)]
34. Urieta-Mora, J.; García-Benito, I.; Molina-Ontoria, A.; Martín, N. Hole transporting materials for perovskite solar cells: A chemical approach. *Chem. Soc. Rev.* **2018**, *47*, 8541–8571. [[CrossRef](#)] [[PubMed](#)]
35. Liu, X.; Zheng, B.; Shi, L.; Zhou, S.; Xu, J.; Liu, Z.; Yun, J.S.; Choi, E.; Zhang, M.; Lv, Y.; et al. Perovskite solar cells based on spiro-OMeTAD stabilized with an alkylthiol additive. *Nat. Photonics* **2023**, *17*, 96–105. [[CrossRef](#)]
36. Pham, N.D.; Shang, J.; Yang, Y.; Hoang, M.T.; Tiong, V.T.; Wang, X.; Fan, L.; Chen, P.; Kou, L.; Wang, L.; et al. Alkaline-earth bis(trifluoromethanesulfonimide) additives for efficient and stable perovskite solar cells. *Nano Energy* **2020**, *69*, 104412. [[CrossRef](#)]
37. Seo, J.-Y.; Kim, H.-S.; Akin, S.; Stojanovic, M.; Simon, E.; Fleischer, M.; Hagfeldt, A.; Zakeeruddin, S.M.; Grätzel, M. Novel p-dopant toward highly efficient and stable perovskite solar cells. *Energy Environ. Sci.* **2018**, *11*, 2985–2992. [[CrossRef](#)]

38. Tan, B.; Raga, S.R.; Chesman, A.S.R.; Furer, S.O.; Zheng, F.; McMeekin, D.P.; Jiang, L.; Mao, W.; Lin, X.; Wen, X.; et al. LiTFSI-Free Spiro-OMeTAD-Based Perovskite Solar Cells with Power Conversion Efficiencies Exceeding 19%. *Adv. Energy Mater.* **2019**, *9*, 1901519. [CrossRef]
39. Kasparavicius, E.; Magomedov, A.; Malinauskas, T.; Getautis, V. Long-Term Stability of the Oxidized Hole-Transporting Materials used in Perovskite Solar Cells. *Chem.—Eur. J.* **2018**, *24*, 9910–9918. [CrossRef]
40. Lamberti, F.; Gatti, T.; Cescon, E.; Sorrentino, R.; Rizzo, A.; Menna, E.; Meneghesso, G.; Meneghetti, M.; Petrozza, A.; Franco, L. Evidence of Spiro-OMeTAD De-doping by tert-Butylpyridine Additive in Hole-Transporting Layers for Perovskite Solar Cells. *Chem* **2019**, *5*, 1806–1817. [CrossRef]
41. Malinauskas, T.; Tomkute-Luksiene, D.; Sens, R.; Daskeviciene, M.; Send, R.; Wonneberger, H.; Jankauskas, V.; Bruder, I.; Getautis, V. Enhancing Thermal Stability and Lifetime of Solid-State Dye-Sensitized Solar Cells via Molecular Engineering of the Hole-Transporting Material Spiro-OMeTAD. *ACS Appl. Mater. Interfaces* **2015**, *7*, 11107–11116. [CrossRef] [PubMed]
42. Lee, I.; Yun, J.H.; Son, H.J.; Kim, T.-S. Accelerated Degradation Due to Weakened Adhesion from Li-TFSI Additives in Perovskite Solar Cells. *ACS Appl. Mater. Interfaces* **2017**, *9*, 7029–7035. [CrossRef] [PubMed]
43. Yun, J.H.; Lee, I.; Kim, T.-S.; Ko, M.J.; Kim, J.Y.; Son, H.J. Synergistic enhancement and mechanism study of mechanical and moisture stability of perovskite solar cells introducing polyethylene-imine into the CH<sub>3</sub>NH<sub>3</sub>PbI<sub>3</sub>/HTM interface. *J. Mater. Chem. A* **2015**, *3*, 22176–22182. [CrossRef]
44. Wei, D.; Wang, T.; Ji, J.; Li, M.; Cui, P.; Li, Y.; Li, G.; Mbengue, J.M.; Song, D. Photo-induced degradation of lead halide perovskite solar cells caused by the hole transport layer/metal electrode interface. *J. Mater. Chem. A* **2016**, *4*, 1991–1998. [CrossRef]
45. Lin, C.-T.; Ngiam, J.; Xu, B.; Chang, Y.-H.; Du, T.; Macdonald, T.J.; Durrant, J.R.; McLachlan, M.A. Enhancing the operational stability of unencapsulated perovskite solar cells through Cu–Ag bilayer electrode incorporation. *J. Mater. Chem. A* **2020**, *8*, 8684–8691. [CrossRef]
46. Jeon, N.J.; Lee, H.G.; Kim, Y.C.; Seo, J.; Noh, J.H.; Lee, J.; Seok, S.I. o-Methoxy Substituents in Spiro-OMeTAD for Efficient Inorganic–Organic Hybrid Perovskite Solar Cells. *J. Am. Chem. Soc.* **2014**, *136*, 7837–7840. [CrossRef]
47. Ashassi-Sorkhabi, H.; Salehi-Abar, P. Design of two novel hole transport materials via replacing the core of spiro-OMeTAD with tetrathiafulvalene and tetraazafulvalene for application in perovskite solar cells. *Sol. Energy* **2018**, *173*, 132–138. [CrossRef]
48. Kadi, Z.; Wang, R.; Berton, N.; Kobeissi, M.; Jiang, Y.; Gao, J.; Schmaltz, B. Interface compatibility: How to outperform classical spiro-OMeTAD in perovskite solar cells with carbazole derivatives. *J. Mater. Chem. C* **2022**, *10*, 7680–7689. [CrossRef]
49. Wu, F.; Wang, B.; Wang, R.; Shan, Y.; Liu, D.; Wong, K.Y.; Chen, T.; Zhu, L. Investigation on a dopant-free hole transport material for perovskite solar cells. *RSC Adv.* **2016**, *6*, 69365–69369. [CrossRef]
50. Xu, B.; Zhang, J.; Hua, Y.; Liu, P.; Wang, L.; Ruan, C.; Li, Y.; Boschloo, G.; Johansson, E.M.J.; Kloo, L.; et al. Tailor-Making Low-Cost Spiro[fluorene-9,9'-xanthene]-Based 3D Oligomers for Perovskite Solar Cells. *Chem* **2017**, *2*, 676–687. [CrossRef]
51. Fu, Y.; Li, Y.; Zeng, Q.; Wu, H.; Wang, L.; Tang, H.; Xing, G.; Cao, D. Influence of donor units on spiro[fluorene-9,9'-xanthene]-based dopant-free hole transporting materials for perovskite solar cells. *Sol. Energy* **2021**, *216*, 180–187. [CrossRef]
52. Bi, D.; Xu, B.; Gao, P.; Sun, L.; Grätzel, M.; Hagfeldt, A. Facile synthesized organic hole transporting material for perovskite solar cell with efficiency of 19.8%. *Nano Energy* **2016**, *23*, 138–144. [CrossRef]
53. Saliba, M.; Orlandi, S.; Matsui, T.; Aghazada, S.; Cavazzini, M.; Correa-Baena, J.-P.; Gao, P.; Scopelliti, R.; Mosconi, E.; Dahmen, K.-H.; et al. A molecularly engineered hole-transporting material for efficient perovskite solar cells. *Nat. Energy* **2016**, *1*, 15017. [CrossRef]
54. Zhang, J.; Xu, B.; Yang, L.; Ruan, C.; Wang, L.; Liu, P.; Zhang, W.; Vlachopoulos, N.; Kloo, L.; Boschloo, G.; et al. The Importance of Pendant Groups on Triphenylamine-Based Hole Transport Materials for Obtaining Perovskite Solar Cells with over 20% Efficiency. *Adv. Energy Mater.* **2018**, *8*, 1701209. [CrossRef]
55. Jeong, M.; Choi, I.W.; Yim, K.; Jeong, S.; Kim, M.; Choi, S.J.; Cho, Y.; An, J.-H.; Kim, H.-B.; Jo, Y.; et al. Large-area perovskite solar cells employing spiro-Naph hole transport material. *Nat. Photonics* **2022**, *16*, 119–125. [CrossRef]
56. Nakka, L.; Cheng, Y.; Aberle, A.G.; Lin, F. Analytical Review of Spiro-OMeTAD Hole Transport Materials: Paths Toward Stable and Efficient Perovskite Solar Cells. *Adv. Energy Sustain. Res.* **2022**, *3*, 2200045. [CrossRef]
57. Li, Y.; Wang, B.; Liu, T.; Zeng, Q.; Cao, D.; Pan, H.; Xing, G. Interfacial Engineering of PTAA/Perovskites for Improved Crystallinity and Hole Extraction in Inverted Perovskite Solar Cells. *ACS Appl. Mater. Interfaces* **2022**, *14*, 3284–3292. [CrossRef]
58. Ko, Y.; Kim, Y.; Lee, C.; Kim, Y.; Jun, Y. Investigation of Hole-Transporting Poly(triarylamine) on Aggregation and Charge Transport for Hysteresisless Scalable Planar Perovskite Solar Cells. *ACS Appl. Mater. Interfaces* **2018**, *10*, 11633–11641. [CrossRef]
59. Noh, J.H.; Im, S.H.; Heo, J.H.; Mandal, T.N.; Seok, S.I. Chemical Management for Colorful, Efficient, and Stable Inorganic–Organic Hybrid Nanostructured Solar Cells. *Nano Lett.* **2013**, *13*, 1764–1769. [CrossRef]
60. Heo, J.H.; Im, S.H.; Noh, J.H.; Mandal, T.N.; Lim, C.-S.; Chang, J.A.; Lee, Y.H.; Kim, H.-j.; Sarkar, A.; Nazeeruddin, M.K.; et al. Efficient inorganic–organic hybrid heterojunction solar cells containing perovskite compound and polymeric hole conductors. *Nat. Photonics* **2013**, *7*, 486–491. [CrossRef]
61. Zhao, Q.; Wu, R.; Zhang, Z.; Xiong, J.; He, Z.; Fan, B.; Dai, Z.; Yang, B.; Xue, X.; Cai, P.; et al. Achieving efficient inverted planar perovskite solar cells with nondoped PTAA as a hole transport layer. *Org. Electron.* **2019**, *71*, 106–112. [CrossRef]
62. Batmunkh, M.; Shearer, C.J.; Biggs, M.J.; Shapter, J.G. Nanocarbons for mesoscopic perovskite solar cells. *J. Mater. Chem. A* **2015**, *3*, 9020–9031. [CrossRef]

63. Lee, I.; Rolston, N.; Brunner, P.-L.; Dauskardt, R.H. Hole-Transport Layer Molecular Weight and Doping Effects on Perovskite Solar Cell Efficiency and Mechanical Behavior. *ACS Appl. Mater. Interfaces* **2019**, *11*, 23757–23764. [[CrossRef](#)] [[PubMed](#)]
64. Brauer, J.C.; Lee, Y.H.; Nazeeruddin, M.K.; Banerji, N. Charge Transfer Dynamics from Organometal Halide Perovskite to Polymeric Hole Transport Materials in Hybrid Solar Cells. *J. Phys. Chem. Lett.* **2015**, *6*, 3675–3681. [[CrossRef](#)] [[PubMed](#)]
65. Khadka, D.B.; Shirai, Y.; Yanagida, M.; Ryan, J.W.; Miyano, K. Exploring the effects of interfacial carrier transport layers on device performance and optoelectronic properties of planar perovskite solar cells. *J. Mater. Chem. C* **2017**, *5*, 8819–8827. [[CrossRef](#)]
66. Yang, W.; Zhong, D.; Shi, M.; Qu, S.; Chen, H. Toward Highly Thermal Stable Perovskite Solar Cells by Rational Design of Interfacial Layer. *iScience* **2019**, *22*, 534–543. [[CrossRef](#)] [[PubMed](#)]
67. Bagheri, Z.; Matteocci, F.; Lamanna, E.; Di Girolamo, D.; Marrani, A.G.; Zanoni, R.; Di Carlo, A.; Moshaii, A. Light-induced improvement of dopant-free PTAA on performance of inverted perovskite solar cells. *Sol. Energy Mater. Sol. Cells* **2020**, *215*, 110606. [[CrossRef](#)]
68. Xia, Y.; Dai, S. Review on applications of PEDOTs and PEDOT:PSS in perovskite solar cells. *J. Mater. Sci. Mater. Electron.* **2021**, *32*, 12746–12757. [[CrossRef](#)]
69. Reza, K.M.; Gurung, A.; Bahrami, B.; Mabrouk, S.; Elbohy, H.; Pathak, R.; Chen, K.; Chowdhury, A.H.; Rahman, M.T.; Letourneau, S.; et al. Tailored PEDOT:PSS hole transport layer for higher performance in perovskite solar cells: Enhancement of electrical and optical properties with improved morphology. *J. Energy Chem.* **2020**, *44*, 41–50. [[CrossRef](#)]
70. Chin, Y.-C.; Daboczi, M.; Henderson, C.; Luke, J.; Kim, J.-S. Suppressing PEDOT:PSS Doping-Induced Interfacial Recombination Loss in Perovskite Solar Cells. *ACS Energy Lett.* **2022**, *7*, 560–568. [[CrossRef](#)]
71. Ha, S.R.; Park, S.; Oh, J.T.; Kim, D.H.; Cho, S.; Bae, S.Y.; Kang, D.-W.; Kim, J.-M.; Choi, H. Water-resistant PEDOT:PSS hole transport layers by incorporating a photo-crosslinking agent for high-performance perovskite and polymer solar cells. *Nanoscale* **2018**, *10*, 13187–13193. [[CrossRef](#)]
72. Xu, D.; Gong, Z.; Jiang, Y.; Feng, Y.; Wang, Z.; Gao, X.; Lu, X.; Zhou, G.; Liu, J.-M.; Gao, J. Constructing molecular bridge for high-efficiency and stable perovskite solar cells based on P3HT. *Nat. Commun.* **2022**, *13*, 7020. [[CrossRef](#)] [[PubMed](#)]
73. De Rossi, F.; Renno, G.; Taheri, B.; Yaghoobi Nia, N.; Ilieva, V.; Fin, A.; Di Carlo, A.; Bonomo, M.; Barolo, C.; Brunetti, F. Modified P3HT materials as hole transport layers for flexible perovskite solar cells. *J. Power Sources* **2021**, *494*, 229735. [[CrossRef](#)]
74. Nia, N.Y.; Matteocci, F.; Cina, L.; Di Carlo, A. High-Efficiency Perovskite Solar Cell Based on Poly(3-Hexylthiophene): Influence of Molecular Weight and Mesoscopic Scaffold Layer. *ChemSusChem* **2017**, *10*, 3854–3860. [[CrossRef](#)] [[PubMed](#)]
75. Wang, J.; Hu, Q.; Li, M.; Shan, H.; Feng, Y.; Xu, Z.-X. Poly(3-hexylthiophene)/Gold Nanorod Composites as Efficient Hole-Transporting Materials for Perovskite Solar Cells. *Sol. RRL* **2020**, *4*, 2000109. [[CrossRef](#)]
76. Li, Y.; Zhang, Y.; Wu, B.; Pang, S.; Yuan, X.; Duan, C.; Huang, F.; Cao, Y. High-Efficiency P3HT-Based All-Polymer Solar Cells with a Thermodynamically Miscible Polymer Acceptor. *Sol. RRL* **2022**, *6*, 2200073. [[CrossRef](#)]
77. Song, J.; Xie, H.; Lim, E.L.; Li, Y.; Kong, T.; Zhang, Y.; Zhou, X.; Duan, C.; Bi, D. Multistrategy Toward Highly Efficient and Stable CsPbI<sub>2</sub>Br Perovskite Solar Cells Based on Dopant-Free Poly(3-Hexylthiophene). *Sol. RRL* **2022**, *6*, 2100880. [[CrossRef](#)]
78. Nayana, V.; Kandasubramanian, B. Polycarbazole and its derivatives: Progress, synthesis, and applications. *J. Polym. Res.* **2020**, *27*, 285. [[CrossRef](#)]
79. Magaldi, D.; Ulfa, M.; Péralta, S.; Goubard, F.; Pauporté, T.; Bui, T.-T. Carbazole-based material: Synthesis, characterization, and application as hole transporting material in perovskite solar cells. *J. Mater. Sci. Mater. Electron.* **2021**, *32*, 12856–12861. [[CrossRef](#)]
80. Wang, C.; Liu, M.; Rahman, S.; Pasanen, H.P.; Tian, J.; Li, J.; Deng, Z.; Zhang, H.; Vivo, P. Hydrogen bonding drives the self-assembling of carbazole-based hole-transport material for enhanced efficiency and stability of perovskite solar cells. *Nano Energy* **2022**, *101*, 107604. [[CrossRef](#)]
81. He, L.; Wang, D.; Zhao, Y.; Zhang, Y.; Wei, W.; Shen, L. Efficient hole transport layers based on cross-linked poly(N-vinylcarbazole) for high-performance perovskite photodetectors. *J. Mater. Chem. C* **2021**, *9*, 11722–11728. [[CrossRef](#)]
82. Kim, G.-W.; Kang, G.; Kim, J.; Lee, G.-Y.; Kim, H.I.; Pyeon, L.; Lee, J.; Park, T. Dopant-free polymeric hole transport materials for highly efficient and stable perovskite solar cells. *Energy Environ. Sci.* **2016**, *9*, 2326–2333. [[CrossRef](#)]
83. Li, M.; Ni, W.; Wan, X.; Zhang, Q.; Kan, B.; Chen, Y. Benzo[1,2-b:4,5-b']dithiophene (BDT)-based small molecules for solution processed organic solar cells. *J. Mater. Chem. A* **2015**, *3*, 4765–4776. [[CrossRef](#)]
84. Yin, X.; Zhou, J.; Song, Z.; Dong, Z.; Bao, Q.; Shrestha, N.; Bista, S.S.; Ellingson, R.J.; Yan, Y.; Tang, W. Dithieno[3,2-b:2',3'-d]pyrrole-Cored Hole Transport Material Enabling Over 21% Efficiency Dopant-Free Perovskite Solar Cells. *Adv. Funct. Mater.* **2019**, *29*, 1904300. [[CrossRef](#)]
85. Zhao, B.X.; Yao, C.; Gu, K.; Liu, T.; Xia, Y.; Loo, Y.-L. A hole-transport material that also passivates perovskite surface defects for solar cells with improved efficiency and stability. *Energy Environ. Sci.* **2020**, *13*, 4334–4343. [[CrossRef](#)]
86. Yu, Z.; Wang, L.; Mu, X.; Chen, C.-C.; Wu, Y.; Cao, J.; Tang, Y. Intramolecular Electric Field Construction in Metal Phthalocyanine as Dopant-Free Hole Transporting Material for Stable Perovskite Solar Cells with >21 % Efficiency. *Angew. Chem. Int. Ed.* **2021**, *60*, 6294–6299. [[CrossRef](#)] [[PubMed](#)]
87. Fu, Q.; Xu, Z.; Tang, X.; Liu, T.; Dong, X.; Zhang, X.; Zheng, N.; Xie, Z.; Liu, Y. Multifunctional Two-Dimensional Conjugated Materials for Dopant-Free Perovskite Solar Cells with Efficiency Exceeding 22%. *ACS Energy Lett.* **2021**, *6*, 1521–1532. [[CrossRef](#)]
88. Lin, H.-S.; Doba, T.; Sato, W.; Matsuo, Y.; Shang, R.; Nakamura, E. Triarylamine/Bithiophene Copolymer with Enhanced Quinoidal Character as Hole-Transporting Material for Perovskite Solar Cells. *Angew. Chem. Int. Ed.* **2022**, *61*, e202203949. [[CrossRef](#)] [[PubMed](#)]



89. Arora, N.; Dar, M.I.; Hinderhofer, A.; Pellet, N.; Schreiber, F.; Zakeeruddin, S.M.; Grätzel, M. Perovskite solar cells with CuSCN hole extraction layers yield stabilized efficiencies greater than 20%. *Science* **2017**, *358*, 768–771. [[CrossRef](#)]
90. Li, R.; Wang, P.; Chen, B.; Cui, X.; Ding, Y.; Li, Y.; Zhang, D.; Zhao, Y.; Zhang, X. NiOx/Spiro Hole Transport Bilayers for Stable Perovskite Solar Cells with Efficiency Exceeding 21%. *ACS Energy Lett.* **2020**, *5*, 79–86. [[CrossRef](#)]
91. Habisreutinger, S.N.; Noel, N.K.; Larson, B.W.; Reid, O.G.; Blackburn, J.L. Rapid Charge-Transfer Cascade through SWCNT Composites Enabling Low-Voltage Losses for Perovskite Solar Cells. *ACS Energy Lett.* **2019**, *4*, 1872–1879. [[CrossRef](#)]
92. Duong, T.; Peng, J.; Walter, D.; Xiang, J.; Shen, H.; Chugh, D.; Lockrey, M.; Zhong, D.; Li, J.; Weber, K.; et al. Perovskite Solar Cells Employing Copper Phthalocyanine Hole-Transport Material with an Efficiency over 20% and Excellent Thermal Stability. *ACS Energy Lett.* **2018**, *3*, 2441–2448. [[CrossRef](#)]
93. Lou, Q.; Lou, G.; Guo, H.; Sun, T.; Wang, C.; Chai, G.; Chen, X.; Yang, G.; Guo, Y.; Zhou, H. Enhanced Efficiency and Stability of n-i-p Perovskite Solar Cells by Incorporation of Fluorinated Graphene in the Spiro-OMeTAD Hole Transport Layer. *Adv. Energy Mater.* **2022**, *12*, 2201344. [[CrossRef](#)]
94. Yin, X.; Song, Z.; Li, Z.; Tang, W. Toward ideal hole transport materials: A review on recent progress in dopant-free hole transport materials for fabricating efficient and stable perovskite solar cells. *Energy Environ. Sci.* **2020**, *13*, 4057–4086. [[CrossRef](#)]
95. Zhang, B.-W.; Lin, H.-S.; Qiu, X.-Y.; Shui, Q.-J.; Zheng, Y.-J.; Almesfer, M.; Kauppinen, E.I.; Matsuo, Y.; Maruyama, S. Spiro-OMeTAD versus PTAA for single-walled carbon nanotubes electrode in perovskite solar cells. *Carbon* **2023**, *205*, 321–327. [[CrossRef](#)]
96. Wassei, J.K.; Kaner, R.B. Graphene, a promising transparent conductor. *Mater. Today* **2010**, *13*, 52–59. [[CrossRef](#)]
97. Chen, D.; Feng, H.; Li, J. Graphene Oxide: Preparation, Functionalization, and Electrochemical Applications. *Chem. Rev.* **2012**, *112*, 6027–6053. [[CrossRef](#)]
98. Razaq, A.; Bibi, F.; Zheng, X.; Papadakis, R.; Jafri, S.H.M.; Li, H. Review on Graphene-, Graphene Oxide-, Reduced Graphene Oxide-Based Flexible Composites: From Fabrication to Applications. *Materials* **2022**, *15*, 1012. [[CrossRef](#)]
99. Naghdi, S.; Sanchez-Arriaga, G.; Rhee, K.Y. Tuning the work function of graphene toward application as anode and cathode. *J. Alloys Compd.* **2019**, *805*, 1117–1134. [[CrossRef](#)]
100. Sygellou, L.; Paterakis, G.; Galiotis, C.; Tasis, D. Work Function Tuning of Reduced Graphene Oxide Thin Films. *J. Phys. Chem. C* **2016**, *120*, 281–290. [[CrossRef](#)]
101. Li, S.-S.; Tu, K.-H.; Lin, C.-C.; Chen, C.-W.; Chhowalla, M. Solution-Processable Graphene Oxide as an Efficient Hole Transport Layer in Polymer Solar Cells. *ACS Nano* **2010**, *4*, 3169–3174. [[CrossRef](#)] [[PubMed](#)]
102. Rafique, S.; Abdullah, S.M.; Shahid, M.M.; Ansari, M.O.; Sulaiman, K. Significantly improved photovoltaic performance in polymer bulk heterojunction solar cells with graphene oxide/PEDOT:PSS double decked hole transport layer. *Sci. Rep.* **2017**, *7*, 39555. [[CrossRef](#)]
103. Yu, J.C.; Jang, J.I.; Lee, B.R.; Lee, G.-W.; Han, J.T.; Song, M.H. Highly Efficient Polymer-Based Optoelectronic Devices Using PEDOT:PSS and a GO Composite Layer as a Hole Transport Layer. *ACS Appl. Mater. Interfaces* **2014**, *6*, 2067–2073. [[CrossRef](#)] [[PubMed](#)]
104. Liu, J.; Xue, Y.; Dai, L. Sulfated Graphene Oxide as a Hole-Extraction Layer in High-Performance Polymer Solar Cells. *J. Phys. Chem. Lett.* **2012**, *3*, 1928–1933. [[CrossRef](#)] [[PubMed](#)]
105. Stratakis, E.; Savva, K.; Konios, D.; Petridis, C.; Kymakis, E. Improving the efficiency of organic photovoltaics by tuning the work function of graphene oxide hole transporting layers. *Nanoscale* **2014**, *6*, 6925–6931. [[CrossRef](#)]
106. Jeon, Y.-J.; Yun, J.-M.; Kim, D.-Y.; Na, S.-I.; Kim, S.-S. Moderately reduced graphene oxide as hole transport layer in polymer solar cells via thermal assisted spray process. *Appl. Surf. Sci.* **2014**, *296*, 140–146. [[CrossRef](#)]
107. Jung, J.W.; Son, S.H.; Choi, J. Polyaniline/Reduced Graphene Oxide Composites for Hole Transporting Layer of High-Performance Inverted Perovskite Solar Cells. *Polymers* **2021**, *13*, 1281. [[CrossRef](#)] [[PubMed](#)]
108. Hong, J.A.; Jung, E.D.; Yu, J.C.; Kim, D.W.; Nam, Y.S.; Oh, I.; Lee, E.; Yoo, J.-W.; Cho, S.; Song, M.H. Improved Efficiency of Perovskite Solar Cells Using a Nitrogen-Doped Graphene-Oxide-Treated Tin Oxide Layer. *ACS Appl. Mater. Interfaces* **2020**, *12*, 2417–2423. [[CrossRef](#)]
109. Soltan, M.S.; Ismail, N.; Hassan, H.M.A.; Shawky, A.; El-Sharkawy, E.A.; Youssef, R.M.; Maruyama, S.; Elshaarawy, R.F.M. Copper nanoparticle-decorated RGO electrodes as hole transport layer of perovskite solar cells enhancing efficiency and shelf stability. *J. Mater. Res. Technol.* **2021**, *14*, 631–638. [[CrossRef](#)]
110. Nicasio-Collazo, J.; Maldonado, J.-L.; Salinas-Cruz, J.; Barreiro-Argüelles, D.; Caballero-Quintana, I.; Vázquez-Espinosa, C.; Romero-Borja, D. Functionalized and reduced graphene oxide as hole transport layer and for use in ternary organic solar cell. *Opt. Mater.* **2019**, *98*, 109434. [[CrossRef](#)]
111. Cheng, X.; Long, J.; Wu, R.; Huang, L.; Tan, L.; Chen, L.; Chen, Y. Fluorinated Reduced Graphene Oxide as an Efficient Hole-Transport Layer for Efficient and Stable Polymer Solar Cells. *ACS Omega* **2017**, *2*, 2010–2016. [[CrossRef](#)] [[PubMed](#)]
112. Yeo, J.-S.; Kang, R.; Lee, S.; Jeon, Y.-J.; Myoung, N.; Lee, C.-L.; Kim, D.-Y.; Yun, J.-M.; Seo, Y.-H.; Kim, S.-S.; et al. Highly efficient and stable planar perovskite solar cells with reduced graphene oxide nanosheets as electrode interlayer. *Nano Energy* **2015**, *12*, 96–104. [[CrossRef](#)]
113. Luo, H.; Lin, X.; Hou, X.; Pan, L.; Huang, S.; Chen, X. Efficient and Air-Stable Planar Perovskite Solar Cells Formed on Graphene-Oxide-Modified PEDOT:PSS Hole Transport Layer. *Nano-Micro Lett.* **2017**, *9*, 39. [[CrossRef](#)]



114. Shin, S.H.; Shin, D.H.; Choi, S.-H. Enhancement of Stability of Inverted Flexible Perovskite Solar Cells by Employing Graphene-Quantum-Dots Hole Transport Layer and Graphene Transparent Electrode Codoped with Gold Nanoparticles and Bis(trifluoromethanesulfonyl)amide. *ACS Sustain. Chem. Eng.* **2019**, *7*, 13178–13185. [[CrossRef](#)]
115. Li, W.; Cheng, N.; Cao, Y.; Zhao, Z.; Xiao, Z.; Zi, W.; Sun, Z. Boost the performance of inverted perovskite solar cells with PEDOT:PSS/Graphene quantum dots composite hole transporting layer. *Org. Electron.* **2020**, *78*, 105575. [[CrossRef](#)]
116. Magne, T.M.; de Oliveira Vieira, T.; Alencar, L.M.R.; Junior, F.F.M.; Gemini-Piperni, S.; Carneiro, S.V.; Fechine, L.M.U.D.; Freire, R.M.; Golokhvast, K.; Metrangolo, P.; et al. Graphene and its derivatives: Understanding the main chemical and medicinal chemistry roles for biomedical applications. *J. Nanostruct. Chem.* **2022**, *12*, 693–727. [[CrossRef](#)] [[PubMed](#)]
117. Li, Y.; Shu, H.; Wang, S.; Wang, J. Electronic and Optical Properties of Graphene Quantum Dots: The Role of Many-Body Effects. *J. Phys. Chem. C* **2015**, *119*, 4983–4989. [[CrossRef](#)]
118. Maheswaran, R.; Shanmugavel, B.P. A Critical Review of the Role of Carbon Nanotubes in the Progress of Next-Generation Electronic Applications. *J. Electron. Mater.* **2022**, *51*, 2786–2800. [[CrossRef](#)]
119. Kalluri, A.; Debnath, D.; Dharmadhikari, B.; Patra, P. Chapter Twelve—Graphene Quantum Dots: Synthesis and Applications. In *Methods Enzymol.*; Kumar, C.V., Ed.; Academic Press: Cambridge, MA, USA, 2018; Volume 609, pp. 335–354.
120. Peng, J.; Gao, W.; Gupta, B.K.; Liu, Z.; Romero-Aburto, R.; Ge, L.; Song, L.; Alemany, L.B.; Zhan, X.; Gao, G.; et al. Graphene Quantum Dots Derived from Carbon Fibers. *Nano Lett.* **2012**, *12*, 844–849. [[CrossRef](#)]
121. Gatou, M.-A.; Vagena, I.-A.; Pippa, N.; Gazouli, M.; Pavlatou, E.A.; Lagopati, N. The Use of Crystalline Carbon-Based Nanomaterials (CBNs) in Various Biomedical Applications. *Crystals* **2023**, *13*, 1236. [[CrossRef](#)]
122. Li, M.; Ni, W.; Kan, B.; Wan, X.; Zhang, L.; Zhang, Q.; Long, G.; Zuo, Y.; Chen, Y. Graphene quantum dots as the hole transport layer material for high-performance organic solar cells. *Phys. Chem. Chem. Phys.* **2013**, *15*, 18973–18978. [[CrossRef](#)]
123. Ali, A.; Kazici, M.; Bozar, S.; Asghar, M.A.; Alwadai, N.; Kahveci, C.; Iqbal, M.; Ahmad, A.; Keskin, B.; Shahbaz, M.; et al. Super aligned carbon nanotubes for interfacial modification of hole transport layer in polymer solar cells. *Sustain. Mater. Technol.* **2023**, *35*, e00569. [[CrossRef](#)]
124. Danish, M.S.S.; Bhattacharya, A.; Stepanova, D.; Mikhaylov, A.; Grilli, M.L.; Khosravy, M.; Senjyu, T. A Systematic Review of Metal Oxide Applications for Energy and Environmental Sustainability. *Metals* **2020**, *10*, 1604. [[CrossRef](#)]
125. Guo, T.; Yao, M.-S.; Lin, Y.-H.; Nan, C.-W. A comprehensive review on synthesis methods for transition-metal oxide nanostructures. *CrystEngComm* **2015**, *17*, 3551–3585. [[CrossRef](#)]
126. Reed, J.; Ceder, G. Role of Electronic Structure in the Susceptibility of Metastable Transition-Metal Oxide Structures to Transformation. *Chem. Rev.* **2004**, *104*, 4513–4534. [[CrossRef](#)] [[PubMed](#)]
127. Qin, P.; He, Q.; Ouyang, D.; Fang, G.; Choy, W.C.H.; Li, G. Transition metal oxides as hole-transporting materials in organic semiconductor and hybrid perovskite based solar cells. *Sci. China Chem.* **2017**, *60*, 472–489. [[CrossRef](#)]
128. Manders, J.R.; Tsang, S.-W.; Hartel, M.J.; Lai, T.-H.; Chen, S.; Amb, C.M.; Reynolds, J.R.; So, F. Solution-Processed Nickel Oxide Hole Transport Layers in High Efficiency Polymer Photovoltaic Cells. *Adv. Funct. Mater.* **2013**, *23*, 2993–3001. [[CrossRef](#)]
129. Zhao, X.; Zhang, W.; Feng, X.; Guo, X.; Lu, C.; Li, X.; Fang, J. Photoconductive NiO<sub>x</sub> hole transport layer for efficient perovskite solar cells. *Chem. Eng. J.* **2022**, *435*, 135140. [[CrossRef](#)]
130. Di Girolamo, D.; Matteocci, F.; Piccinni, M.; Di Carlo, A.; Dini, D. Anodically electrodeposited NiO nanoflakes as hole selective contact in efficient air processed p-i-n perovskite solar cells. *Sol. Energy Mater. Sol. Cells* **2020**, *205*, 110288. [[CrossRef](#)]
131. Sun, J.; Lu, J.; Li, B.; Jiang, L.; Chesman, A.S.R.; Scully, A.D.; Gengenbach, T.R.; Cheng, Y.-B.; Jasieniak, J.J. Inverted perovskite solar cells with high fill-factors featuring chemical bath deposited mesoporous NiO hole transporting layers. *Nano Energy* **2018**, *49*, 163–171. [[CrossRef](#)]
132. Chen, W.; Wu, Y.; Fan, J.; Djurišić, A.B.; Liu, F.; Tam, H.W.; Ng, A.; Surya, C.; Chan, W.K.; Wang, D.; et al. Understanding the Doping Effect on NiO: Toward High-Performance Inverted Perovskite Solar Cells. *Adv. Energy Mater.* **2018**, *8*, 1703519. [[CrossRef](#)]
133. Li, G.; Jiang, Y.; Deng, S.; Tam, A.; Xu, P.; Wong, M.; Kwok, H.-S. Overcoming the Limitations of Sputtered Nickel Oxide for High-Efficiency and Large-Area Perovskite Solar Cells. *Adv. Sci.* **2017**, *4*, 1700463. [[CrossRef](#)] [[PubMed](#)]
134. Yates, H.M.; Meroni, S.M.P.; Raptis, D.; Hodgkinson, J.L.; Watson, T.M. Flame assisted chemical vapour deposition NiO hole transport layers for mesoporous carbon perovskite cells. *J. Mater. Chem. C* **2019**, *7*, 13235–13242. [[CrossRef](#)]
135. Parthiban, S.; Kim, S.; Tamilavan, V.; Lee, J.; Shin, I.; Yuvaraj, D.; Jung, Y.K.; Hyun, M.H.; Jeong, J.H.; Park, S.H. Enhanced efficiency and stability of polymer solar cells using solution-processed nickel oxide as hole transport material. *Curr. Appl. Phys.* **2017**, *17*, 1232–1237. [[CrossRef](#)]
136. Kim, J.K. PEG-assisted Sol-gel Synthesis of Compact Nickel Oxide Hole-Selective Layer with Modified Interfacial Properties for Organic Solar Cells. *Polymers* **2019**, *11*, 120. [[CrossRef](#)]
137. Xu, L.; Chen, X.; Jin, J.; Liu, W.; Dong, B.; Bai, X.; Song, H.; Reiss, P. Inverted perovskite solar cells employing doped NiO hole transport layers: A review. *Nano Energy* **2019**, *63*, 103860. [[CrossRef](#)]
138. Liu, Z.; Chang, J.; Lin, Z.; Zhou, L.; Yang, Z.; Chen, D.; Zhang, C.; Liu, S.; Hao, Y. High-Performance Planar Perovskite Solar Cells Using Low Temperature, Solution-Combustion-Based Nickel Oxide Hole Transporting Layer with Efficiency Exceeding 20%. *Adv. Energy Mater.* **2018**, *8*, 1703432. [[CrossRef](#)]
139. Boyd, C.C.; Shallcross, R.C.; Moot, T.; Kerner, R.; Bertoluzzi, L.; Onno, A.; Kavadiya, S.; Chosy, C.; Wolf, E.J.; Werner, J.; et al. Overcoming Redox Reactions at Perovskite-Nickel Oxide Interfaces to Boost Voltages in Perovskite Solar Cells. *Joule* **2020**, *4*, 1759–1775. [[CrossRef](#)]

140. Huang, S.; Wang, Y.; Shen, S.; Tang, Y.; Yu, A.; Kang, B.; Silva, S.R.P.; Lu, G. Enhancing the performance of polymer solar cells using solution-processed copper doped nickel oxide nanoparticles as hole transport layer. *J. Colloid Interface Sci.* **2019**, *535*, 308–317. [[CrossRef](#)]
141. Ouyang, D.; Zheng, J.; Huang, Z.; Zhu, L.; Choy, W.C.H. An efficacious multifunction codoping strategy on a room-temperature solution-processed hole transport layer for realizing high-performance perovskite solar cells. *J. Mater. Chem. A* **2021**, *9*, 371–379. [[CrossRef](#)]
142. Wan, X.; Jiang, Y.; Qiu, Z.; Zhang, H.; Zhu, X.; Sikandar, I.; Liu, X.; Chen, X.; Cao, B. Zinc as a New Dopant for NiO<sub>x</sub>-Based Planar Perovskite Solar Cells with Stable Efficiency near 20%. *ACS Appl. Energy Mater.* **2018**, *1*, 3947–3954. [[CrossRef](#)]
143. Saki, Z.; Sveinbjörnsson, K.; Boschloo, G.; Taghavinia, N. The Effect of Lithium Doping in Solution-Processed Nickel Oxide Films for Perovskite Solar Cells. *ChemPhysChem* **2019**, *20*, 3322–3327. [[CrossRef](#)] [[PubMed](#)]
144. He, J.; Xiang, Y.; Zhang, F.; Lian, J.; Hu, R.; Zeng, P.; Song, J.; Qu, J. Improvement of red light harvesting ability and open circuit voltage of Cu:NiO<sub>x</sub> based p-i-n planar perovskite solar cells boosted by cysteine enhanced interface contact. *Nano Energy* **2018**, *45*, 471–479. [[CrossRef](#)]
145. Chavhan, S.D.; Hansson, R.; Ericsson, L.K.E.; Beyer, P.; Hofmann, A.; Brütting, W.; Opitz, A.; Moons, E. Low temperature processed NiO<sub>x</sub> hole transport layers for efficient polymer solar cells. *Org. Electron.* **2017**, *44*, 59–66. [[CrossRef](#)]
146. Jiang, F.; Choy, W.C.H.; Li, X.; Zhang, D.; Cheng, J. Post-treatment-Free Solution-Processed Non-stoichiometric NiO<sub>x</sub> Nanoparticles for Efficient Hole-Transport Layers of Organic Optoelectronic Devices. *Adv. Mater.* **2015**, *27*, 2930–2937. [[CrossRef](#)] [[PubMed](#)]
147. Liu, Y.-F.; Zhang, S.-W.; Li, Y.-X.; Li, S.-L.; Huang, L.-Q.; Jing, Y.-N.; Cheng, Q.; Xiao, L.-G.; Wang, B.-X.; Han, B.; et al. Solution-processed Molybdenum Oxide Hole Transport Layer Stabilizes Organic Solar Cells. *Chin. J. Polym. Sci.* **2023**, *41*, 202–211. [[CrossRef](#)]
148. Pan, W.; Tian, R.; Jin, H.; Guo, Y.; Zhang, L.; Wu, X.; Zhang, L.; Han, Z.; Liu, G.; Li, J.; et al. Structure, Optical, and Catalytic Properties of Novel Hexagonal Metastable h-MoO<sub>3</sub> Nano- and Microrods Synthesized with Modified Liquid-Phase Processes. *Chem. Mater.* **2010**, *22*, 6202–6208. [[CrossRef](#)]
149. Jasieniak, J.J.; Seiffter, J.; Jo, J.; Mates, T.; Heeger, A.J. A Solution-Processed MoO<sub>x</sub> Anode Interlayer for Use within Organic Photovoltaic Devices. *Adv. Funct. Mater.* **2012**, *22*, 2594–2605. [[CrossRef](#)]
150. Yang, B.; Chen, Y.; Cui, Y.; Liu, D.; Xu, B.; Hou, J. Over 100-nm-Thick MoO<sub>x</sub> Films with Superior Hole Collection and Transport Properties for Organic Solar Cells. *Adv. Energy Mater.* **2018**, *8*, 1800698. [[CrossRef](#)]
151. Han, S.; Shin, W.S.; Seo, M.; Gupta, D.; Moon, S.-J.; Yoo, S. Improving performance of organic solar cells using amorphous tungsten oxides as an interfacial buffer layer on transparent anodes. *Org. Electron.* **2009**, *10*, 791–797. [[CrossRef](#)]
152. Chen, C.; Jiang, Y.; Wu, Y.; Guo, J.; Kong, X.; Wu, X.; Li, Y.; Zheng, D.; Wu, S.; Gao, X.; et al. Low-Temperature-Processed WO<sub>x</sub> as Electron Transfer Layer for Planar Perovskite Solar Cells Exceeding 20% Efficiency. *Sol. RRL* **2020**, *4*, 1900499. [[CrossRef](#)]
153. Hussain, S.; Liu, H.; Hussain, M.; Mehran, M.T.; Kim, H.-S.; Jung, J.; Vikraman, D.; Kang, J. Development of MXene/WO<sub>3</sub> embedded PEDOT:PSS hole transport layers for highly efficient perovskite solar cells and X-ray detectors. *Int. J. Energy Res.* **2022**, *46*, 12485–12497. [[CrossRef](#)]
154. Shen, W.; Tang, J.; Wang, D.; Yang, R.; Chen, W.; Bao, X.; Wang, Y.; Jiao, J.; Wang, Y.; Huang, Z.; et al. Enhanced efficiency of polymer solar cells by structure-differentiated silver nano-dopants in solution-processed tungsten oxide layer. *Mater. Sci. Eng. B* **2016**, *206*, 61–68. [[CrossRef](#)]
155. Liu, P.; Wang, C.; Zhou, D.; Yuan, Q.; Wang, Y.; Hu, Y.; Han, D.; Feng, L. WO<sub>x</sub>@PEDOT Core-Shell Nanorods: Hybrid Hole-Transporting Materials for Efficient and Stable Perovskite Solar Cells. *ACS Appl. Energy Mater.* **2018**, *1*, 1742–1752. [[CrossRef](#)]
156. Ali, F.; Pham, N.D.; Fan, L.; Tiong, V.; Ostrikov, K.; Bell, J.M.; Wang, H.; Tesfamichael, T. Low Hysteresis Perovskite Solar Cells Using an Electron-Beam Evaporated WO<sub>3-x</sub> Thin Film as the Electron Transport Layer. *ACS Appl. Energy Mater.* **2019**, *2*, 5456–5464. [[CrossRef](#)]
157. Wang, K.; Shi, Y.; Dong, Q.; Li, Y.; Wang, S.; Yu, X.; Wu, M.; Ma, T. Low-Temperature and Solution-Processed Amorphous WO<sub>x</sub> as Electron-Selective Layer for Perovskite Solar Cells. *J. Phys. Chem. Lett.* **2015**, *6*, 755–759. [[CrossRef](#)]
158. Liu, C.; Zhou, X.; Chen, S.; Zhao, X.; Dai, S.; Xu, B. Hydrophobic Cu<sub>2</sub>O Quantum Dots Enabled by Surfactant Modification as Top Hole-Transport Materials for Efficient Perovskite Solar Cells. *Adv. Sci.* **2019**, *6*, 1801169. [[CrossRef](#)]
159. Tan, W.; Hendricks, O.L.; Meng, A.C.; Braun, M.R.; McGehee, M.D.; Chidsey, C.E.D.; McIntyre, P.C. Atomic Layer Deposited TiO<sub>2</sub>-IrO<sub>x</sub> Alloy as a Hole Transport Material for Perovskite Solar Cells. *Adv. Mater. Interfaces* **2018**, *5*, 1800191. [[CrossRef](#)]
160. Yang, B.; Ouyang, D.; Huang, Z.; Ren, X.; Zhang, H.; Choy, W.C.H. Multifunctional Synthesis Approach of In:CuCrO<sub>2</sub> Nanoparticles for Hole Transport Layer in High-Performance Perovskite Solar Cells. *Adv. Funct. Mater.* **2019**, *29*, 1902600. [[CrossRef](#)]
161. Huang, Z.; Ouyang, D.; Ma, R.; Wu, W.; Roy, V.A.L.; Choy, W.C.H. A General Method: Designing a Hypocrystalline Hydroxide Intermediate to Achieve Ultrasmall and Well-Dispersed Ternary Metal Oxide for Efficient Photovoltaic Devices. *Adv. Funct. Mater.* **2019**, *29*, 1904684. [[CrossRef](#)]
162. Papadas, I.T.; Ioakeimidis, A.; Armatas, G.S.; Choulis, S.A. Low-Temperature Combustion Synthesis of a Spinel NiCo<sub>2</sub>O<sub>4</sub> Hole Transport Layer for Perovskite Photovoltaics. *Adv. Sci.* **2018**, *5*, 1701029. [[CrossRef](#)]
163. Bashir, A.; Shukla, S.; Lew, J.H.; Shukla, S.; Bruno, A.; Gupta, D.; Baikie, T.; Patidar, R.; Akhter, Z.; Priyadarshi, A.; et al. Spinel Co<sub>3</sub>O<sub>4</sub> nanomaterials for efficient and stable large area carbon-based printed perovskite solar cells. *Nanoscale* **2018**, *10*, 2341–2350. [[CrossRef](#)]

164. Yu, Z.; Liu, W.; Fu, W.; Zhang, Z.; Yang, W.; Wang, S.; Li, H.; Xu, M.; Chen, H. An aqueous solution-processed  $\text{CuO}_x$  film as an anode buffer layer for efficient and stable organic solar cells. *J. Mater. Chem. A* **2016**, *4*, 5130–5136. [[CrossRef](#)]
165. Yu, R.-S.; Tasi, C.-P. Structure, composition and properties of p-type  $\text{CuCrO}_2$  thin films. *Ceram. Int.* **2014**, *40*, 8211–8217. [[CrossRef](#)]
166. Han, M.; Jiang, K.; Zhang, J.; Yu, W.; Li, Y.; Hu, Z.; Chu, J. Structural, electronic band transition and optoelectronic properties of delafossite  $\text{CuGa}_{1-x}\text{Cr}_x\text{O}_2$  ( $0 \leq x \leq 1$ ) solid solution films grown by the sol–gel method. *J. Mater. Chem.* **2012**, *22*, 18463–18470. [[CrossRef](#)]
167. Xiong, D.; Xu, Z.; Zeng, X.; Zhang, W.; Chen, W.; Xu, X.; Wang, M.; Cheng, Y.-B. Hydrothermal synthesis of ultrasmall  $\text{CuCrO}_2$  nanocrystal alternatives to  $\text{NiO}$  nanoparticles in efficient p-type dye-sensitized solar cells. *J. Mater. Chem.* **2012**, *22*, 24760–24768. [[CrossRef](#)]
168. Wang, J.; Daunis, T.B.; Cheng, L.; Zhang, B.; Kim, J.; Hsu, J.W.P. Combustion Synthesis of p-Type Transparent Conducting  $\text{CuCrO}_{2+x}$  and  $\text{Cu:CrO}_x$  Thin Films at 180 °C. *ACS Appl. Mater. Interfaces* **2018**, *10*, 3732–3738. [[CrossRef](#)]
169. Zhang, B.; Thampy, S.; Dunlap-Shohl, W.A.; Xu, W.; Zheng, Y.; Cao, F.-Y.; Cheng, Y.-J.; Malko, A.V.; Mitzi, D.B.; Hsu, J.W.P. Mg Doped  $\text{CuCrO}_2$  as Efficient Hole Transport Layers for Organic and Perovskite Solar Cells. *Nanomaterials* **2019**, *9*, 1311. [[CrossRef](#)]
170. Wang, Y.; Djurišić, A.B.; Chen, W.; Liu, F.; Cheng, R.; Ping Feng, S.; Ng, A.M.C.; He, Z. Metal oxide charge transport layers in perovskite solar cells—Optimising low temperature processing and improving the interfaces towards low temperature processed, efficient and stable devices. *J. Phys. Energy* **2021**, *3*, 012004. [[CrossRef](#)]
171. Yang, X.; Liang, H.-J.; Yu, H.-Y.; Wang, M.-Y.; Zhao, X.-X.; Wang, X.-T.; Wu, X.-L. Recent progresses and challenges of metal sulfides as advanced anode materials in rechargeable sodium-ion batteries. *J. Phys. Mater.* **2020**, *3*, 042004. [[CrossRef](#)]
172. Chen, J.; Chua, D.H.C.; Lee, P.S. The Advances of Metal Sulfides and In Situ Characterization Methods beyond Li Ion Batteries: Sodium, Potassium, and Aluminum Ion Batteries. *Small Methods* **2020**, *4*, 1900648. [[CrossRef](#)]
173. Pariari, D.; Sarma, D.D. Nature and origin of unusual properties in chemically exfoliated 2D  $\text{MoS}_2$ . *APL Mater.* **2020**, *8*, 040909. [[CrossRef](#)]
174. Ray, S.C. Structure and optical properties of molybdenum disulphide ( $\text{MoS}_2$ ) thin film deposited by the dip technique. *J. Mater. Sci. Lett.* **2000**, *19*, 803–804. [[CrossRef](#)]
175. Frey, G.L.; Tenne, R.; Matthews, M.J.; Dresselhaus, M.S.; Dresselhaus, G. Optical Properties of  $\text{MS}_2$  ( $M = \text{Mo}, \text{W}$ ) Inorganic Fullerenelike and Nanotube Material Optical Absorption and Resonance Raman Measurements. *J. Mater. Res.* **1998**, *13*, 2412–2417. [[CrossRef](#)]
176. Tan, C.; Zhang, H. Two-dimensional transition metal dichalcogenide nanosheet-based composites. *Chem. Soc. Rev.* **2015**, *44*, 2713–2731. [[CrossRef](#)]
177. Huang, X.; Zeng, Z.; Zhang, H. Metal dichalcogenide nanosheets: Preparation, properties and applications. *Chem. Soc. Rev.* **2013**, *42*, 1934–1946. [[CrossRef](#)]
178. Kumar, N.; Tomar, R.; Wadehra, N.; Devi, M.M.; Prakash, B.; Chakraverty, S. Growth of Highly Crystalline and Large Scale Monolayer  $\text{MoS}_2$  by CVD: The Role of substrate Position. *Cryst. Res. Technol.* **2018**, *53*, 1800002. [[CrossRef](#)]
179. Li, Y.; Li, Y.-L.; Araujo, C.M.; Luo, W.; Ahuja, R. Single-layer  $\text{MoS}_2$  as an efficient photocatalyst. *Catal. Sci. Technol.* **2013**, *3*, 2214–2220. [[CrossRef](#)]
180. Hu, X.; Zeng, X.; Liu, Y.; Lu, J.; Yuan, S.; Yin, Y.; Hu, J.; McCarthy, D.T.; Zhang, X. Nano-layer based 1T-rich  $\text{MoS}_2/\text{g-C}_3\text{N}_4$  co-catalyst system for enhanced photocatalytic and photoelectrochemical activity. *Appl. Catal. B* **2019**, *268*, 118466. [[CrossRef](#)]
181. He, Q.; Wang, L.; Yin, K.; Luo, S. Vertically Aligned Ultrathin 1T- $\text{WS}_2$  Nanosheets Enhanced the Electrocatalytic Hydrogen Evolution. *Nanoscale Res. Lett.* **2018**, *13*, 167. [[CrossRef](#)]
182. Liu, H.; Wu, R.; Tian, L.; Kong, Y.; Sun, Y. Synergetic photocatalytic effect between 1 T@2H- $\text{MoS}_2$  and plasmon resonance induced by Ag quantum dots. *Nanotechnology* **2018**, *29*, 285402. [[CrossRef](#)]
183. Yang, D.; Jimenez Sandoval, S.; Divigalpitiya, W.M.R.; Frindt, R.F. Structure of single-molecular-layer  $\text{MoS}_2$ . *Phys. Rev. B* **1991**, *43*, 12053. [[CrossRef](#)]
184. Li, X.; Zhu, H. Two-dimensional  $\text{MoS}_2$ : Properties, preparation, and applications. *J. Mater.* **2015**, *1*, 33–44. [[CrossRef](#)]
185. Liang, M.; Ali, A.; Belaidi, A.; Hossain, M.I.; Ronan, O.; Downing, C.; Tabet, N.; Sanvito, S.; Ei-Mellouhi, F.; Nicolosi, V. Improving stability of organometallic-halide perovskite solar cells using exfoliation two-dimensional molybdenum chalcogenides. *NPJ 2D Mater. Appl.* **2020**, *4*, 40. [[CrossRef](#)]
186. Wang, D.; Elumalai, N.K.; Mahmud, M.A.; Yi, H.; Upama, M.B.; Lee Chin, R.A.; Conibeer, G.; Xu, C.; Haque, F.; Duan, L.; et al.  $\text{MoS}_2$  incorporated hybrid hole transport layer for high performance and stable perovskite solar cells. *Synth. Met.* **2018**, *246*, 195–203. [[CrossRef](#)]
187. Le, Q.V.; Nguyen, T.P.; Jang, H.W.; Kim, S.Y. The use of UV/ozone-treated  $\text{MoS}_2$  nanosheets for extended air stability in organic photovoltaic cells. *Phys. Chem. Chem. Phys.* **2014**, *16*, 13123–13128. [[CrossRef](#)] [[PubMed](#)]
188. Le, Q.V.; Nguyen, T.P.; Kim, S.Y. UV/ozone-treated  $\text{WS}_2$  hole-extraction layer in organic photovoltaic cells. *Phys. Status Solidi-Rapid Res. Lett.* **2014**, *8*, 390–394. [[CrossRef](#)]
189. Le, Q.V.; Nguyen, T.P.; Choi, K.S.; Cho, Y.H.; Hong, Y.J.; Kim, S.Y. Dual use of tantalum disulfides as hole and electron extraction layers in organic photovoltaic cells. *Phys. Chem. Chem. Phys.* **2014**, *16*, 25468–25472. [[CrossRef](#)] [[PubMed](#)]
190. Martinez-Rojas, F.; Hssein, M.; El Jouad, Z.; Armijo, F.; Cattin, L.; Louarn, G.; Stephant, N.; del Valle, M.A.; Addou, M.; Soto, J.P.; et al.  $\text{Mo}(\text{S}_x\text{O}_y)$  thin films deposited by electrochemistry for application in organic photovoltaic cells. *Mater. Chem. Phys.* **2017**, *201*, 331–338. [[CrossRef](#)]
191. Xing, W.; Chen, Y.; Wang, X.; Lv, L.; Ouyang, X.; Ge, Z.; Huang, H.  $\text{MoS}_2$  Quantum Dots with a Tunable Work Function for High-Performance Organic Solar Cells. *ACS Appl. Mater. Interfaces* **2016**, *8*, 26916–26923. [[CrossRef](#)]



192. Adilbekova, B.; Lin, Y.; Yengel, E.; Faber, H.; Harrison, G.; Firdaus, Y.; El-Labban, A.; Anjum, D.H.; Tung, V.; Anthopoulos, T.D. Liquid phase exfoliation of MoS<sub>2</sub> and WS<sub>2</sub> in aqueous ammonia and their application in highly efficient organic solar cells. *J. Mater. Chem. C* **2020**, *8*, 5259–5264. [[CrossRef](#)]
193. Van Le, Q.; Nguyen, T.P.; Park, M.; Sohn, W.; Jang, H.W.; Kim, S.Y. Bottom-Up Synthesis of MeS<sub>x</sub>Nanodots for Optoelectronic Device Applications. *Adv. Opt. Mater.* **2016**, *4*, 1796–1804. [[CrossRef](#)]
194. Le, Q.V.; Kim, C.M.; Nguyen, T.P.; Park, M.; Kim, T.-Y.; Han, S.M.; Kim, S.Y. (NH<sub>4</sub>)<sub>2</sub>WS<sub>4</sub> precursor as a hole-injection layer in organic optoelectronic devices. *Chem. Eng. J.* **2016**, *284*, 285–293. [[CrossRef](#)]
195. Rao, H.; Sun, W.; Ye, S.; Yan, W.; Li, Y.; Peng, H.; Liu, Z.; Bian, Z.; Huang, C. Solution-Processed CuS NPs as an Inorganic Hole-Selective Contact Material for Inverted Planar Perovskite Solar Cells. *ACS Appl. Mater. Interfaces* **2016**, *8*, 7800–7805. [[CrossRef](#)]
196. Li, J.; Wang, Y.; Zang, S.; Pan, D.; Zhang, X.; Liu, Y. CuS<sub>x</sub> hole transport layer for PbS quantum dot solar cell. *Sol. Energy* **2020**, *209*, 118–122. [[CrossRef](#)]
197. Tirado, J.; Roldán-Carmona, C.; Muñoz-Guerrero, F.A.; Bonilla-Arboleda, G.; Ralaiarisoa, M.; Grancini, G.; Queloz, V.I.E.; Koch, N.; Nazeeruddin, M.K.; Jaramillo, F. Copper sulfide nanoparticles as hole-transporting-material in a fully-inorganic blocking layers n-i-p perovskite solar cells: Application and working insights. *Appl. Surf. Sci.* **2019**, *478*, 607–614. [[CrossRef](#)]
198. Peng, Z.; Luo, W.; Long, C.; Wang, Y.; Fu, Y. A Cu<sub>x</sub>S/GO composite hole transport layer for photovoltaic performance enhancement on CuInS<sub>2</sub> quantum dot-sensitized solar cells. *Appl. Phys. A* **2022**, *129*, 54. [[CrossRef](#)]
199. Kumar, P.; You, S.; Vomiero, A. CuSCN as a hole transport layer in an inorganic solution-processed planar Sb<sub>2</sub>S<sub>3</sub> solar cell, enabling carbon-based and semitransparent photovoltaics. *J. Mater. Chem. C* **2022**, *10*, 16273–16282. [[CrossRef](#)]
200. Suresh Kumar, M.; Mohanta, K.; Batabyal, S.K. Solution processed Cu<sub>2</sub>CdSnS<sub>4</sub> as a low-cost inorganic hole transport material for polymer solar cells. *Sol. Energy Mater. Sol. Cells* **2017**, *161*, 157–161. [[CrossRef](#)]
201. Yu, Z.; Li, W.; Cheng, N.; Liu, Z.; Lei, B.; Xiao, Z.; Zi, W.; Zhao, Z.; Tu, Y. Cu<sub>2</sub>SnS<sub>3</sub> Nanocrystal-Based Hole-Transport Layer for Carbon Electrode-Based Perovskite Solar Cells. *ACS Appl. Nano Mater.* **2022**, *5*, 10755–10762. [[CrossRef](#)]
202. Molla, A.; Sahu, M.; Hussain, S. Synthesis of Tunable Band Gap Semiconductor Nickel Sulphide Nanoparticles: Rapid and Round the Clock Degradation of Organic Dyes. *Sci. Rep.* **2016**, *6*, 26034. [[CrossRef](#)]
203. Hamed, M.S.G.; Oseni, S.O.; Kumar, A.; Sharma, G.; Mola, G.T. Nickel sulphide nano-composite assisted hole transport in thin film polymer solar cells. *Sol. Energy* **2020**, *195*, 310–317. [[CrossRef](#)]
204. Hilal, M.; Han, J.I. Preparation of hierarchical flower-like nickel sulfide as hole transporting material for organic solar cells via a one-step solvothermal method. *Sol. Energy* **2019**, *188*, 403–413. [[CrossRef](#)]
205. Pitchaiya, S.; Natarajan, M.; Santhanam, A.; Ramakrishnan, V.M.; Asokan, V.; Palanichamy, P.; Rangasamy, B.; Sundaram, S.; Velauthapillai, D. Nickel sulphide-carbon composite hole transporting material for (CH<sub>3</sub>NH<sub>3</sub>PbI<sub>3</sub>) planar heterojunction perovskite solar cell. *Mater. Lett.* **2018**, *221*, 283–288. [[CrossRef](#)]
206. He, Z.; Zhou, Y.; Liu, A.; Gao, L.; Zhang, C.; Wei, G.; Ma, T. Recent progress in metal sulfide-based electron transport layers in perovskite solar cells. *Nanoscale* **2021**, *13*, 17272–17289. [[CrossRef](#)]
207. Arumugam, G.M.; Karunakaran, S.K.; Liu, C.; Zhang, C.; Guo, F.; Wu, S.; Mai, Y. Inorganic hole transport layers in inverted perovskite solar cells: A review. *Nano Sel.* **2021**, *2*, 1081–1116. [[CrossRef](#)]
208. Guo, J.-J.; Bai, Z.-C.; Meng, X.-F.; Sun, M.-M.; Song, J.-H.; Shen, Z.-S.; Ma, N.; Chen, Z.-L.; Zhang, F. Novel dopant-free metallophthalocyanines based hole transporting materials for perovskite solar cells: The effect of core metal on photovoltaic performance. *Sol. Energy* **2017**, *155*, 121–129. [[CrossRef](#)]
209. Wang, J.-M.; Wang, Z.-K.; Li, M.; Zhang, C.-C.; Jiang, L.-L.; Hu, K.-H.; Ye, Q.-Q.; Liao, L.-S. Doped Copper Phthalocyanine via an Aqueous Solution Process for Normal and Inverted Perovskite Solar Cells. *Adv. Energy Mater.* **2018**, *8*, 1701688. [[CrossRef](#)]
210. Liu, X.; Liu, Z.; Sun, B.; Tan, X.; Ye, H.; Tu, Y.; Shi, T.; Tang, Z.; Liao, G. 17.46% efficient and highly stable carbon-based planar perovskite solar cells employing Ni-doped rutile TiO<sub>2</sub> as electron transport layer. *Nano Energy* **2018**, *50*, 201–211. [[CrossRef](#)]
211. Cui, Z.; Wang, Y.; Chen, Y.; Chen, X.; Deng, X.; Chen, W.; Shi, C. Soluble tetra-methoxytriphenylamine substituted zinc phthalocyanine as dopant-free hole transporting materials for perovskite solar cells. *Org. Electron.* **2019**, *69*, 248–254. [[CrossRef](#)]
212. Cheng, M.; Li, Y.; Safdari, M.; Chen, C.; Liu, P.; Kloo, L.; Sun, L. Efficient Perovskite Solar Cells Based on a Solution Processable Nickel(II) Phthalocyanine and Vanadium Oxide Integrated Hole Transport Layer. *Adv. Energy Mater.* **2017**, *7*, 1602556. [[CrossRef](#)]
213. Chen, S.; Liu, P.; Hua, Y.; Li, Y.; Kloo, L.; Wang, X.; Ong, B.; Wong, W.-K.; Zhu, X. Study of Arylamine-Substituted Porphyrins as Hole-Transporting Materials in High-Performance Perovskite Solar Cells. *ACS Appl. Mater. Interfaces* **2017**, *9*, 13231–13239. [[CrossRef](#)] [[PubMed](#)]
214. Cao, J.; Lv, X.; Zhang, P.; Chuong, T.T.; Wu, B.; Feng, X.; Shan, C.; Liu, J.; Tang, Y. Plant Sunscreen and Co(II)/(III) Porphyrins for UV-Resistant and Thermally Stable Perovskite Solar Cells: From Natural to Artificial. *Adv. Mater.* **2018**, *30*, 1800568. [[CrossRef](#)]
215. Chen, R.; Feng, Y.; Zhang, C.; Wang, M.; Jing, L.; Ma, C.; Bian, J.; Shi, Y. Carbon-based HTL-free modular perovskite solar cells with improved contact at perovskite/carbon interfaces. *J. Mater. Chem. C* **2020**, *8*, 9262–9270. [[CrossRef](#)]
216. Stubhan, T.; Li, N.; Luechinger, N.A.; Halim, S.C.; Matt, G.J.; Brabec, C.J. High Fill Factor Polymer Solar Cells Incorporating a Low Temperature Solution Processed WO<sub>3</sub> Hole Extraction Layer. *Adv. Energy Mater.* **2012**, *2*, 1433–1438. [[CrossRef](#)]
217. Kim, G.; Min, H.; Lee, K.S.; Lee, D.Y.; Yoon, S.M.; Seok, S.I. Impact of strain relaxation on performance of  $\alpha$ -formamidinium lead iodide perovskite solar cells. *Science* **2020**, *370*, 108–112. [[CrossRef](#)]

218. Gu, X.; Lai, X.; Zhang, Y.; Wang, T.; Tan, W.L.; McNeill, C.R.; Liu, Q.; Sonar, P.; He, F.; Li, W.; et al. Organic Solar Cell With Efficiency Over 20% and VOC Exceeding 2.1 V Enabled by Tandem With All-Inorganic Perovskite and Thermal Annealing-Free Process. *Adv. Sci.* **2022**, *9*, 2200445. [[CrossRef](#)]
219. Zheng, Z.; Wang, J.; Bi, P.; Ren, J.; Wang, Y.; Yang, Y.; Liu, X.; Zhang, S.; Hou, J. Tandem Organic Solar Cell with 20.2% Efficiency. *Joule* **2022**, *6*, 171–184. [[CrossRef](#)]
220. Ullah, F.; Chen, C.-C.; Choy, W.C.H. Recent Developments in Organic Tandem Solar Cells toward High Efficiency. *Adv. Energy Sustain. Res.* **2021**, *2*, 2000050. [[CrossRef](#)]
221. Solak, E.K.; Irmak, E. Advances in organic photovoltaic cells: A comprehensive review of materials, technologies, and performance. *RSC Adv.* **2023**, *13*, 12244–12269. [[CrossRef](#)]
222. Gebremichael, Z.T.; Ugokwe, C.; Alam, S.; Stumpf, S.; Diegel, M.; Schubert, U.S.; Hoppe, H. How varying surface wettability of different PEDOT:PSS formulations and their mixtures affects perovskite crystallization and the efficiency of inverted perovskite solar cells. *RSC Adv.* **2022**, *12*, 25593–25604. [[CrossRef](#)]
223. Wang, S.; Cabreros, A.; Yang, Y.; Hall, A.S.; Valenzuela, S.; Luo, Y.; Correa-Baena, J.-P.; Kim, M.-c.; Fjeldberg, Ø.; Fenning, D.P.; et al. Impacts of the Hole Transport Layer Deposition Process on Buried Interfaces in Perovskite Solar Cells. *Cell Rep. Phys. Sci.* **2020**, *1*, 100103. [[CrossRef](#)]
224. Chaudhary, N.; Naqvi, S.; Rathore, D.; Rathi, S.; Patra, A. Solvent influenced morphology control of hole transport layer of CuSCN on performance of organic solar cells. *Mater. Chem. Phys.* **2022**, *282*, 125898. [[CrossRef](#)]
225. Wang, S.; Sina, M.; Parikh, P.; Uekert, T.; Shahbazian, B.; Devaraj, A.; Meng, Y.S. Role of 4-tert-Butylpyridine as a Hole Transport Layer Morphological Controller in Perovskite Solar Cells. *Nano Lett.* **2016**, *16*, 5594–5600. [[CrossRef](#)] [[PubMed](#)]
226. Pham, V.T.H.; Trinh, T.K.; Shaikh, H.M.; Al-Zahrani, S.M.; Alhamidi, A.; Bin Dahman, S.; Tamboli, M.S.; Truong, N.T.N. Controlling of Conductivity and Morphological Properties of Hole-Transport Layer Using Ionic Liquid for Vacuum-Free Planar Hybrid Solar Cells. *Energies* **2023**, *16*, 467. [[CrossRef](#)]

**Disclaimer/Publisher's Note:** The statements, opinions and data contained in all publications are solely those of the individual author(s) and contributor(s) and not of MDPI and/or the editor(s). MDPI and/or the editor(s) disclaim responsibility for any injury to people or property resulting from any ideas, methods, instructions or products referred to in the content.